THULIUM FIBER LASER LITHOTRIPSY

by

Richard Leious Blackmon, Jr.

A dissertation submitted to the faculty of
The University of North Carolina at Charlotte
in partial fulfillment of the requirements
for the degree of Doctor of Philosophy in
Optical Science and Engineering

Charlotte

2013

Approved by:

_____
Dr. Nathaniel Fried

_____
Dr. Gregory Gbur

_____
Dr. Ana Jofre

_____
Dr. Susan Trammell

_____
Dr. James Conrad

©2013
Richard Leious Blackmon, Jr.
ALL RIGHTS RESERVED

ABSTRACT

RICHARD LEIOUS BLACKMON, JR. Thulium fiber laser lithotripsy (Under the direction of DR. NATHANIEL FRIED)

The Thulium Fiber Laser (TFL) has been studied as a potential alternative to the conventional Holmium:YAG laser (Ho:YAG) for the treatment of kidney stones. The TFL is more ideally suited for laser lithotripsy because of the higher absorption coefficient of the emitted wavelength in water, the superior Gaussian profile of the laser beam, and the ability to operate at arbitrary temporal pulse profiles. The higher absorption of the TFL by water helps translate into higher ablation of urinary stones using less energy. The Gaussian spatial beam profile allows the TFL to couple into fibers much smaller than those currently being used for Ho:YAG lithotripsy. Lastly, the ability of arbitrary pulse operation by the TFL allows energy to be delivered to the stone efficiently so as to avoid negative effects (such as burning or bouncing of the stone) while maximizing ablation. Along with these improvements, the unique properties of the TFL have led to more novel techniques that have currently not been used in the clinic, such as the ability to control the movement of stones based on the manner in which the laser energy is delivered. Lastly, the TFL has led to the development of novel fibers, such as the tapered fiber and removable tip fiber, to be used for lithotripsy which can lead to safer and less expensive treatment of urinary stones. Overall, the TFL has been demonstrated as a viable alternative to the conventional Ho:YAG laser and has the potential to advance methods and tools for treatment of kidney stones.

DEDICATION

This dissertation is dedicated to my loving grandmother. She has been an ongoing source of inspiration and support. Her guidance and experience has been the foundation on which I have built my education. Without her, I would have not reached this significant milestone in my life.

ACKNOWLEDGMENTS

This research was supported, in part, by a Collaborative Research Grant between UNC-Charlotte and the Carolinas Medical Center, and a Faculty Research Grant from UNC-Charlotte. I was supported by a National Science Foundation Graduate Fellowship.

I wish to thank Nancy Tresser of Imalux, inc. (Cleveland, OH) for the optical coherence tomography system used in this study and Louis C Herring (Orlando, FL) and LabCorp (Oklahoma City, OK) for providing the human urinary stone samples used in these studies. I also thank Dr. Pierce Irby of McKay Urology at Carolinas Medical Center for providing some of the ureteroscope equipment used in these studies as well as his valuable clinical advice, Jason Case and Dr. Susan Trammell for assistance with the temperature studies, and Thomas Hutchens for the design of and assistance with the detachable fiber tip studies.

TABLE OF CONTENTS

LIST OF FIGURES

LIST OF TABLES

LIST OF ABBREVIATIONS

COM	calcium oxalate monohydrate
CW	continuous wave
Ho:YAG	holmium: yttrium aluminum garnet
MPT	micro-pulse train
OCT	optical coherence tomography
OD	outer diameter
PoP	plaster of paris
S.D.	standard deviation
TFL	thulium fiber laser
UA	uric acid
YAG	yttrium aluminum garnet

CHAPTER 1: INTRODUCTION

1.1 Urinary Stone Disease

Kidney stone disease is a common and costly disorder in the United States. Up to 12 percent of males and 7 percent of females are affected during their lifetime [1]. Estimates of annual costs to the national health care system reach $5.3 billion. Each year, over 3 million patient visits to health care providers occur with over 500,000 treatments in emergency rooms for kidney stone problems [2].

When the body lacks proper hydration, crystalline structures form in the urinary tract. In particular, the high heat and humidity and high salt diet in the southeastern U.S. has led this region to be referred to as the "stone belt." The southeast U.S. has nearly twice the prevalence of urinary stones than the northwestern U.S [3]. Furthermore, recent global warming studies also predict significant climate-related increases in stone disease in the coming decades, including a 10% increase in prevalence and 25% increase in costs [4].

A significant percentage of kidney stone presentations require surgical intervention. Figure 1 shows the percentages of all urinary stones formed in the urinary tract. Uric acid and calcium oxylate stones account for 80.3% of urinary stones formed. Calcium Phosphate and Struvite stones account for 18.2% of stones formed. These stones can be chemically dissolved and are typically treated with drug therapy. The remaining 1.5% are very difficult to break up with a laser so other treatments are used for

these stones. Therefore, we have concentrated our study on the majority of stones that are typically treated with lasers, COM and UA.

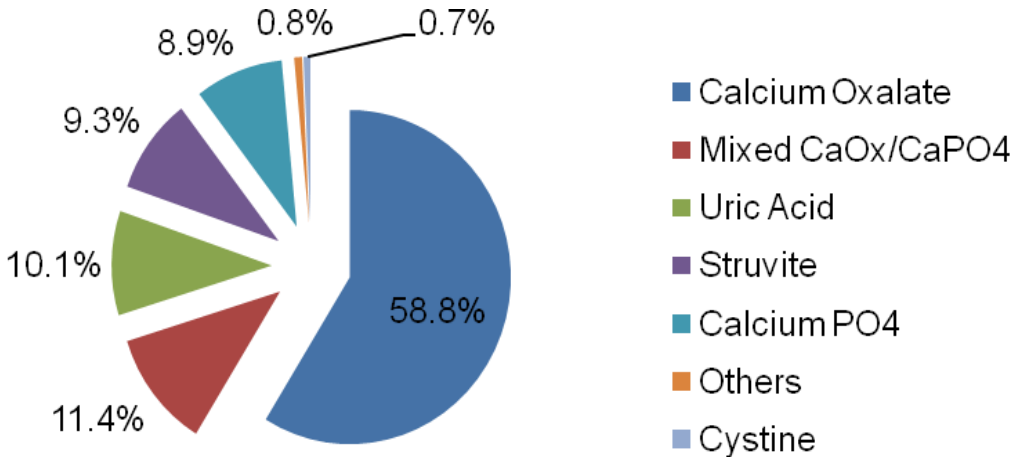

Figure 1. Pie chart showing percentage of urinary stones formed [5].

Laser lithotripsy, predominantly via advanced ureteroscopy, has become a major technique for the minimally invasive surgical destruction of bladder, ureter, and kidney stones. For small to moderate sized or multiple urinary stones, this technology is the preferred surgical option over extracorporeal shock wave lithotripsy in many centers in the U.S. Maximal clinical efficiency of laser lithotripsy is important to decrease operative time, surgical risk, and costs. The rate of stone destruction, or ablation rate, is a significant measure of efficiency. Laser energy tends to propel stones backward (resulting in retropulsion) from the optical fiber tip unless the stone is fixed or impacted by surrounding tissues within the ureter or kidney. Retropulsion is a clinically significant

phenomenon, as it causes the surgeon to “chase” the stone, resulting in a decrease in ablation efficiency and increase in surgical time. Thus, less retropulsion would be a desirable feature of a laser lithotripter.

1.2 Holmium:YAG laser lithotripsy

The solid-state Holmium:YAG laser (Ho:YAG) has become the principal laser lithotripter in clinical use over the past 15 years. It is used in part because there is relatively high water absorption at the emission wavelength of 2120 nm. The Ho:YAG laser is also the preferred laser among urologists because it can be used for multiple applications, including cutting and coagulation of a variety of soft and hard tissues. The high water absorption is necessary in ablating stone tissue because the urinary stone has a significant bound water component and is typically immersed in a urine or saline environment during the lithotripsy procedure. The Ho:YAG laser is typically operated with pulse energies of 0.5-2 J, a 350-700 μs pulse duration, pulse repetition rates of 10-20 Hz, and average powers of 10-20 W.

While useful in allowing surgeons to treat kidney stone disease in an endoscopic approach, the Ho:YAG laser has many limitations. Although the clinical flashlamp-pumped Ho:YAG laser is capable of operating at high pulse energies, it is limited to operation at relatively low pulse repetition rates (10-20 Hz) during lithotripsy due to thermal lensing effects in the laser rod [6]. To achieve higher pulse repetition rates, multiple laser heads must be combined. This significantly increases the cost and complexity of the Ho:YAG laser [6].

High pulse energies (0.5-2 J) must be used to achieve sufficient ablation rates using the low pulse rate clinical Ho:YAG laser. This may cause significant retropulsion

of the kidney stones [7-12]. When retropulsion occurs, stones can become lost or migrate from the ureter to deep inside the kidney. The surgeon must then find the stone again before continuing ablation. This increases the time needed to ablate the stone and also increases the chance of complications during the procedure. Therefore, it is important to minimize stone retropulsion during laser lithotripsy.

Low-OH, multimode silica optical fibers with core diameters ranging from 150-1000 μm are commercially available for use with the Ho:YAG laser during lithotripsy procedures. However, the Ho:YAG laser multimode beam profile (Figure 2) prohibits coupling of high laser powers into small-core fibers, without risking overfilling of the input fiber core, launching into the cladding, and damage to the fiber. Typical Ho:YAG laser beam diameters measure 275-500 μm [13], significantly larger than the 150-200 μm core fibers that urologists wish to use during laser lithotripsy procedures in hard-to-reach locations such as the lower pole of the kidney. Not only is the probability of fiber failure higher during extreme bending with these larger and less flexible fibers, but another problem is presented when using these fibers. During laser lithotripsy, saline irrigation is flushed through the same working port as occupied by the fiber. Poor visibility during laser lithotripsy is due to the creation of stone particles in the field-of-view. Frequent saline irrigation of the working area is necessary; however, irrigation rates can be significantly lowered by the use of larger fibers which fill up a larger cross-section of the working port.

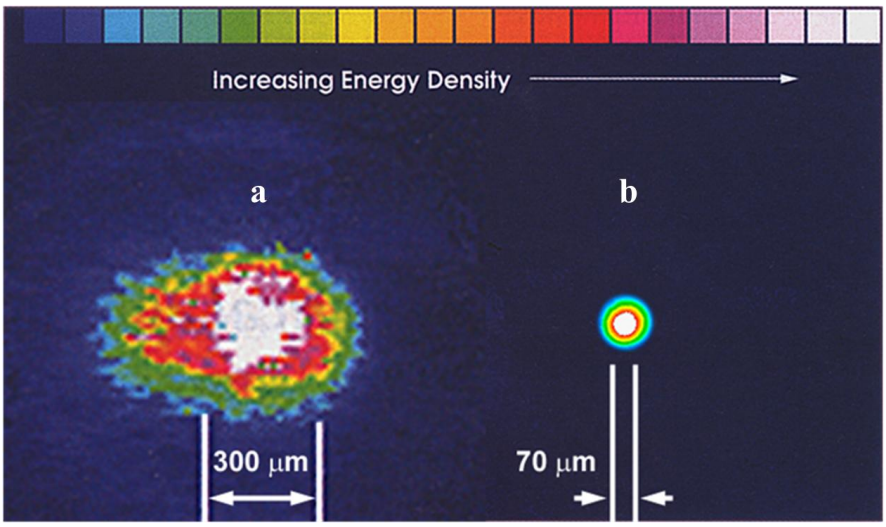

Figure 2. Spatial beam profiles for (a) Ho:YAG laser (300 μm) on the left, and (b) TFL (70 μm) on the right. Unlike the TFL beam, the multimode Ho:YAG laser beam typically overflows 150 and 200 μm core fibers used during laser lithotripsy in the lower pole of the kidney (Figure adapted from [13]).

1.3 Thulium fiber laser lithotripsy

The Thulium fiber laser (TFL) is a logical choice for study as an alternative laser lithotripter to that of the Ho:YAG laser. The TFL has two major emission wavelengths at 1908 and 1940 nm. Unlike the Ho:YAG laser wavelength (2120 nm), these two TFL wavelengths closely match both a high- and low-temperature water absorption peak in tissue, respectively (Figure 3). As water heats up during laser ablation, the water absorption peak shifts to a shorter wavelength from about 1940 nm at room temperature to about 1910 nm at ablation temperatures [14-16]. Water is the primary absorber of laser radiation in both soft and hard tissues in the near- and mid-infrared part of the spectrum. Soft tissues have approximately 60-70% water content and hard tissues have approximately 20-30% water content. The water absorption coefficient at 2120 nm measures 2.5 mm^{-1}, resulting in a penetration depth of 400 μm, while the absorption

coefficient in the 1908-1940 nm wavelength range measures approximately 15 mm^{-1}, resulting in a penetration depth of about 70 μm. This shorter penetration depth should translate into a lower ablation threshold and more efficient laser tissue ablation for the TFL compared with the Ho:YAG laser [17].

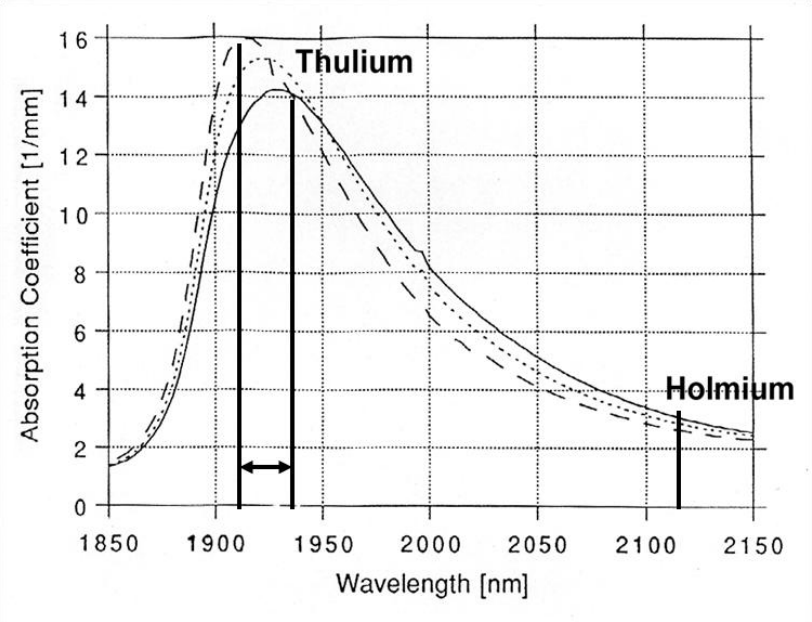

Figure 3. A low-temperature water absorption peak is 1940 nm which shifts to about 1910 nm at higher temperatures. The central emission lines of the TFL at 1908 and 1940 nm match this peak more closely than the Ho:YAG laser (2120 nm), which should translate into more efficient ablation of soft and hard tissues. (Figure adapted from [15]).

The TFL used in this study was modulated with a function generator. This allowed for greater flexibility in pulse duration and pulse repetition rate. Futhermore, the temporal pulse profile is more uniform compared to that of the Ho:YAG laser (shown in Figure 4). A disadvantage to modulation is that much of the power is wasted and the shorter pulse duration yields a lower pulse energy. The loss of pulse energy is

compensated for in part by operation at higher pulse repetition rates. The TFL is able to operate at 1-1000 Hz. This research demonstrates that operation at low pulse energy with higher pulse repetition rates reduces retropulsion.

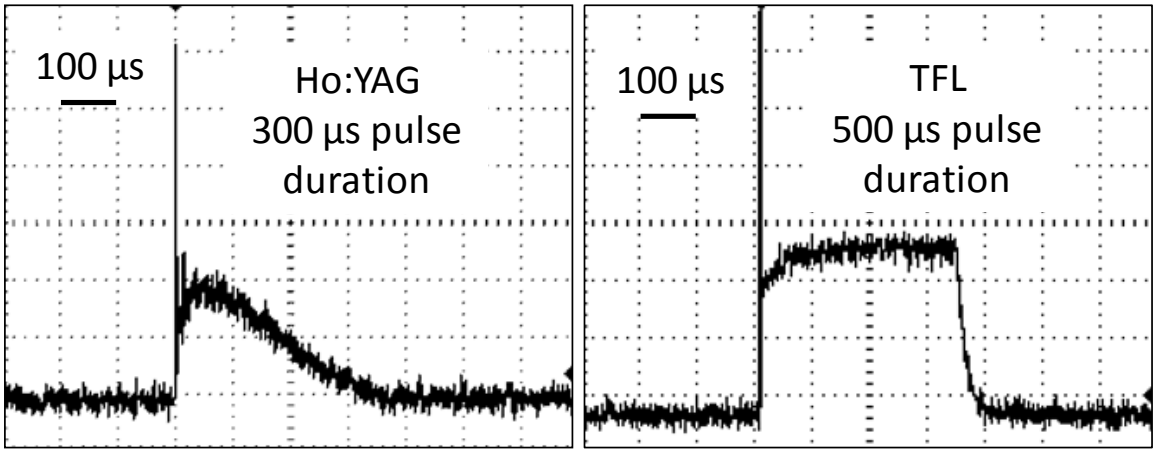

Figure 4. Temporal pulse profiles of the Ho:YAG and TFL.

In addition, one of the primary advantages of fiber laser technology is the excellent spatial beam profile as compared to the multimode beam of solid-state lasers. The improved spatial beam profile of a fiber laser (Figure 2b) should eliminate the concerns that currently plague Ho:YAG laser lithotripsy, including overfilling of the input fiber, inefficient fiber coupling, and thermal lensing effects. This allows use of smaller fibers during lithotripsy. Smaller fibers in turn allow for increased flexibility of the endoscope and increased saline irrigation rates. A greater ability to navigate through the kidney and irrigate the treatment area may result in less procedure time, greater safety, and a less expensive operation.

CHAPTER 2: URINARY STONE ABLATION

2.1 Introduction

Stone ablation rate is defined as the mass of stone removal per unit time (µg/s). One method to increase ablation rates is to increase the energy delivered in each pulse. The limitation of this approach is that it leads to an increase in retropulsion. Another method to increase the ablation rate is to increase the pulse duration. Increasing the pulse duration beyond the thermal relaxation time is inefficient because thermal confinement is no longer achieved and some of the energy delivered to the stone is not used in the ablation process, but rather diffuses out of the treatment area and into the surrounding stone, exhibiting itself in the form of char on the stone surface. The char layer then sticks to the fiber tip and accelerates the process of fiber tip degradation. Another method of increasing the ablation rate is to increase the laser pulse repetition rate. Increasing the laser pulse rate is ideal because the pulse energy can then be decreased while theoretically maintaining ablation rates and thus reducing retropulsion typically caused by high pulse energies.

Unfortunately, the Ho:YAG laser ablation rate is typically increased by increasing the pulse energy, resulting in stone fragmentation at the expense of an increase in retropulsion. While the ablation rate is increased when the fiber is in contact with the stone, actual procedure time may be longer because of the time wasted continuously chasing the stone in the urinary tract. The Ho:YAG ablation rate can also be increased by

increasing the pulse repetition rate to a certain extent, but this is limited by thermal lensing effects in the laser rod due to the inefficient flashlamp-pumped design of the Ho:YAG laser. Ho:YAG lasers operating at up to 50 Hz are commercially available, but are significantly more expensive, as they typically consist of four laser cavities combined into one system. For example, a standard Ho:YAG laser operating at 20 Hz and 20 Watts may cost approximately $60,000 while a 50 Hz, 100 Watt laser may cost about $150,000.

TFL ablation rates can be increased by increasing pulse duration and/or pulse rates. Increasing pulse duration enables delivery of higher pulse energy but results in charring as shown in Figure 5. Charring is a result of excess heat causing desiccation and burning, rather than ablation, from loss of thermal confinement. To maintain thermal confinement and thus eliminate charring, operation at pulse durations less than the value of the thermal relaxation time is necessary. Thermal confinement for urinary stones was calculated using the general equation $\tau = \delta^2/4K$, where τ is thermal relaxation time, δ is the optical penetration depth of laser energy, and K is thermal diffusivity. Thermal diffusivity is defined by $K = \kappa/\rho c$, where κ is thermal conductivity, ρ is stone density, and c is specific heat. Since these thermal properties are unknown for urinary stones, thermal relaxation times were calculated using other representative hard tissue models. For bone, the thermal relaxation time is calculated to be 8.4 ms [18]. For calcified plaque, thermal relaxation times vary between 5.9-7.7 ms (0% to 20% water content) [19]. In Figure 5, significant stone char is observed at laser pulse durations of 5 ms and greater, consistent with these calculated thermal relaxation times.

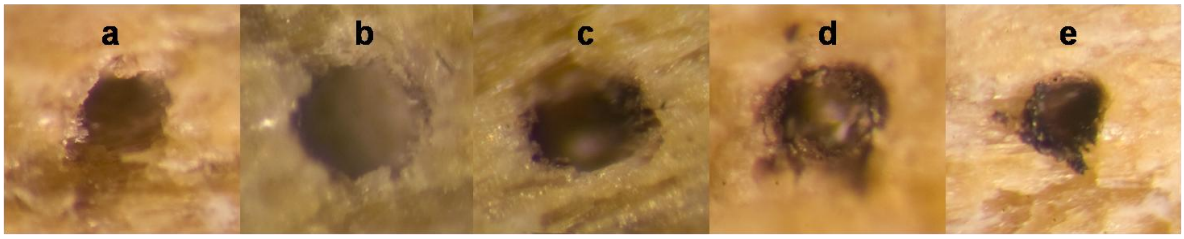

Figure 5. Ablation craters in uric acid samples created with Thulium fiber laser at varying pulse durations (2 pulses at 70 mJ / pulse): (a) 1 ms; (b) 2 ms; (c) 5 ms; (d) 10 ms; (e) 20 ms. Charring increases as the laser pulse duration increases.

Maintaining thermal confinement requires operating at pulse durations below the thermal relaxation time. A disadvantage of limiting the pulse duration with the TFL is the sacrifice of pulse energy. For example, a 100 W TFL operating with a pulse duration of 500 μs, the highest theoretical pulse energy from the laser is ~50 mJ. After accounting for reflection losses at each interface of the lens and fiber, this number drops to approximately 37 mJ. However, the TFL is capable of achieving pulse rates of up to 1000 Hz, which may compensate for the use of these low pulse energies.

The ablation threshold is defined as the lowest incident fluence (energy per unit area) per pulse at which stone material is removed. When performing sensitive experiments on kidney stones, it is important to know the ablation threshold. Experiments must be performed well above the ablation threshold to obtain rapid tissue removal rates. Our studies have found previous reports of Ho:YAG ablation thresholds to be significantly lower than measured in our laboratory. Furthermore, TFL ablation thresholds have not yet been determined. Therefore, we have conducted experiments to determine what the ablation threshold is for both the Ho:YAG and TFL for the two most common types of urinary stones treated with lasers, uric acid and calcium oxalate monohydrate. This is critical in determining the best parameters for subsequent studies.

2.2 Methods

A clinical Holmium:YAG laser (TwoPointOne XE, Coherent, Santa Clara, CA) was operated with a wavelength of 2120 nm, variable pulse energies from 5-165 mJ (low pulse energies achieved using attenuators), 300-µs pulse duration, and a pulse rate of 10 Hz. For comparison, an experimental TFL (TLR 110-1908, IPG Photonics, inc., Oxford, MA) was externally modulated with a function generator (Model DS345, Stanford Research Systems, Sunnyvale, CA) to operate in pulsed mode with a wavelength of 1908 nm, pulse energies of 5-35 mJ, 500-µs pulse duration, and pulse rates ranging from 10-100 Hz.

Human calcium oxalate monohydrate (COM) and uric acid (UA) urinary stone samples with masses of 200-1100 mg, and of purity greater than 95% were obtained from two stone analysis laboratories (Louis C. Herring & Co, Orlando, FL and Labcorp, Oklahoma City, OK) and used for this study. The stone samples were held fixed and submerged in a saline bath. For each laser, the pulse rate was fixed at 10 Hz, and a fixed number of 6000 pulses were delivered through 200-µm-core optical fibers (BFL22-200, Thorlabs, Newton, NJ) in contact mode with the stone. The pulse energy was escalated in small increments until stone mass loss could be measured, using an analytical balance (AB54-S, Mettler-Toledo, Switzerland). Total mass loss measurements less than 1 mg were considered to be within experimental error and negligible. This would translate into a mass loss of less than 1 µg/pulse compared to orders of magnitude higher mass loss per pulse typically encountered in the clinic during laser lithotripsy. There was also no visual confirmation of ablation for values below this number. The ablation threshold was then determined by plotting mass loss (mg) versus fluence (J/cm^2) with a linear fit to the data.

The coefficient of determination (R^2) is shown to describe how well the line fits the data. The x-intercept of this fit determined the ablation threshold value. Ablation rates were plotted versus pulse energy for the Ho:YAG and pulse rate for the TFL.

2.3 Results and Discussion

2.3.1 Ablation Thresholds

Mass loss versus fluence using the Ho:YAG laser was plotted for COM stones in Figure 6 and UA stones in Figure 7. Mass loss versus fluence using the TFL was plotted for COM stones in Figure 8 and UA stones in Figure 9. All graphs show a highly linear fit to the data points. The COM stone ablation threshold for the Ho:YAG and TFL measured 82.6 J/cm^2 and 20.8 J/cm^2, respectively. The UA stone ablation threshold for Ho:YAG and TFL measured 25.9 J/cm^2 and 6.5 J/cm^2 respectively. The slopes of the plots are similar for each stone composition. This illustrates that for both lasers there is a similar increase in mass loss per unit increase in fluence.

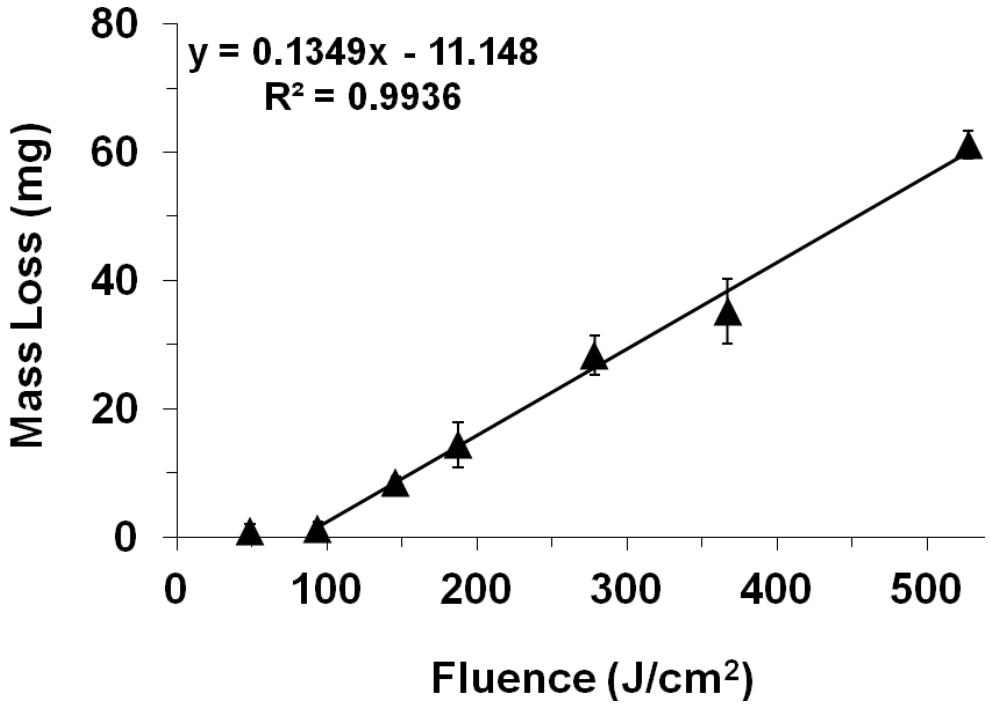

Figure 6. Plot of amount of COM stone removal versus fluence using the Ho:YAG.

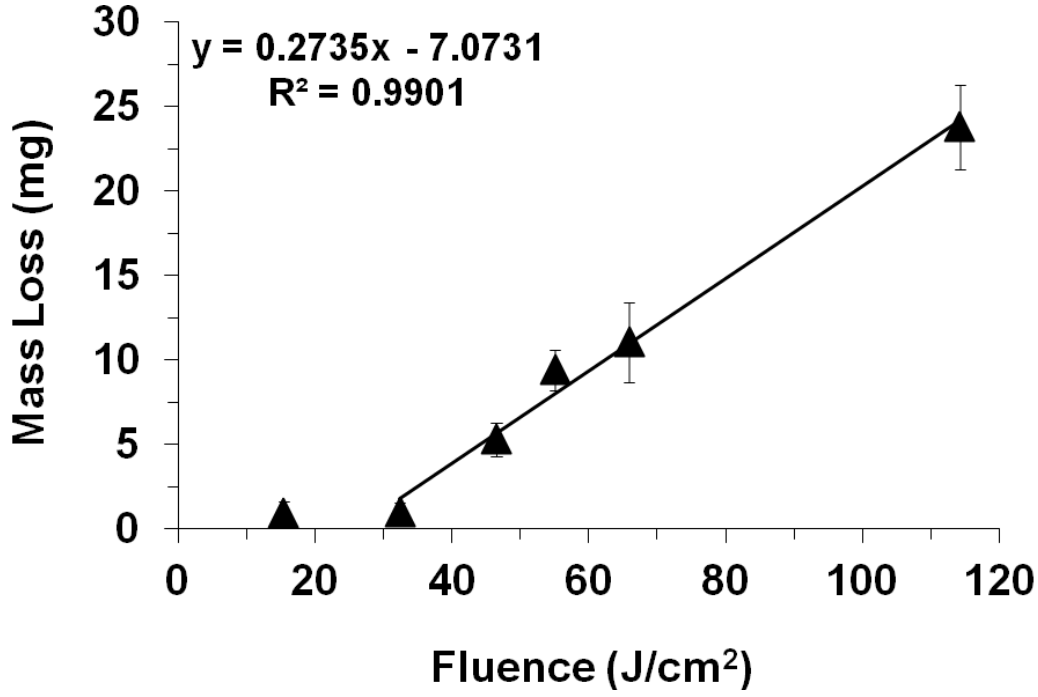

Figure 7. Plot of amount of UA stone removal versus fluence for Ho:YAG.

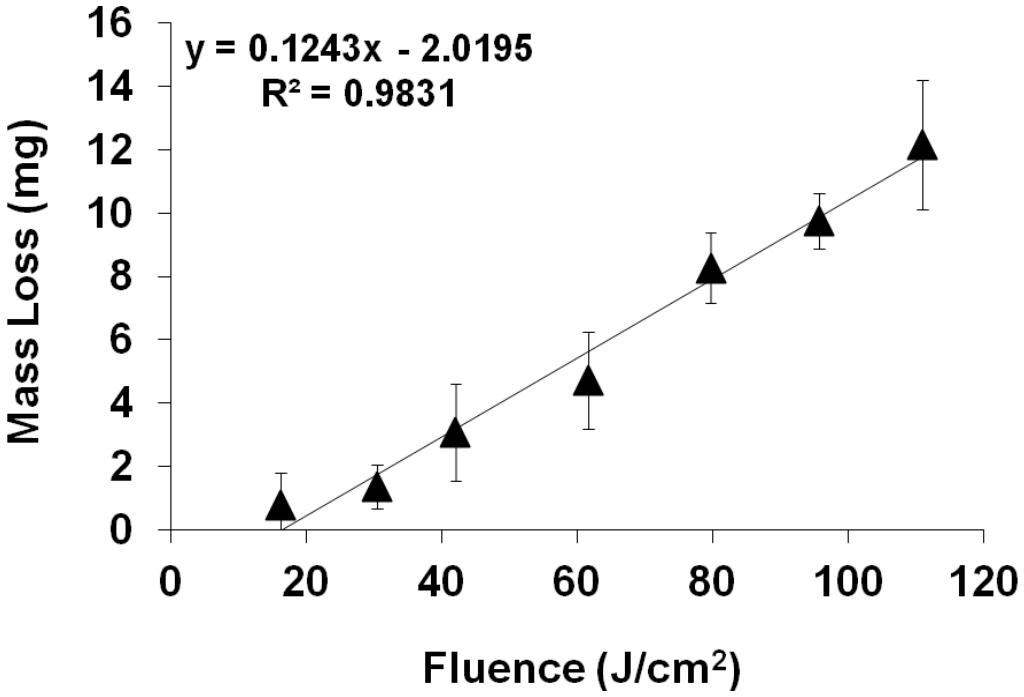

Figure 8. Plot of amount of COM stone removal versus fluence using the TFL.

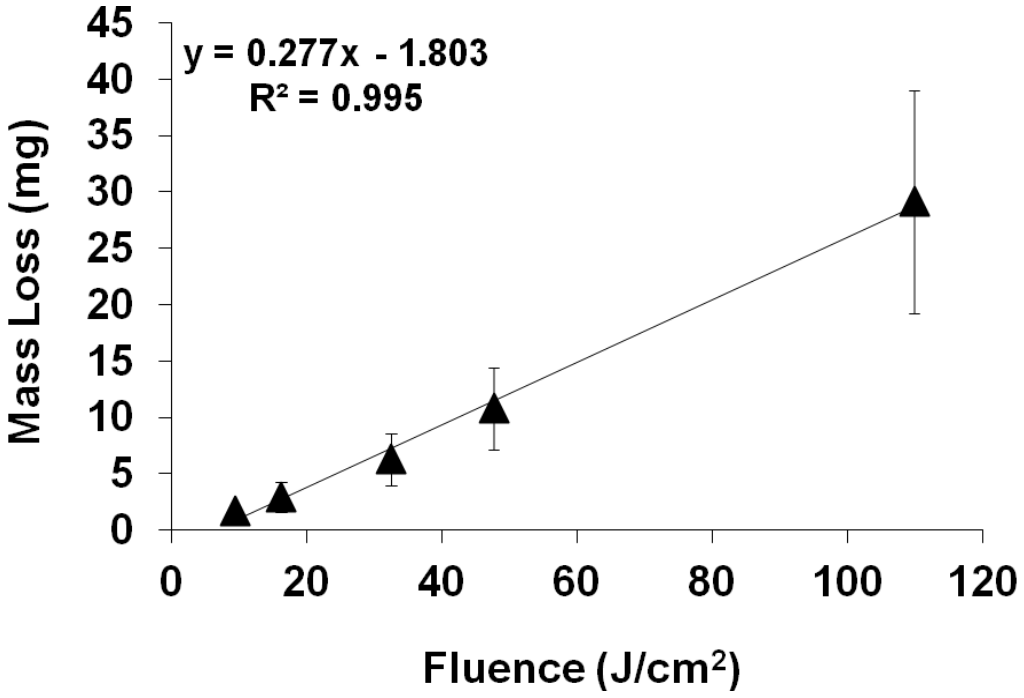

Figure 9. Plot of amount of UA stone removal versus fluence using TFL.

It should be noted that the COM ablation threshold for the Ho:YAG laser (82.6 J/cm^2) is an order of magnitude higher than the value of 7.36 J/cm^2, previously reported [20]. Similarly, the UA ablation threshold for the Ho:YAG laser (25.9 J/cm^2) is also significantly higher than the value of 3.72 J/cm^2, previously reported [20]. The difference in reported ablation threshold values may be due to several factors. First, ablation thresholds were measured using different criteria in the two studies: by recording smallest measurable mass loss over many (6000) pulses in our study compared with visual confirmation of smallest mass loss observable for a single pulse in previous study. Second, a Free-Electron Laser (FEL) was used to determine stone ablation thresholds in the previous study, which has a unique temporal pulse structure (macropulse of 3-5 μs consisting of picosecond micropulses) that is significantly different than that of the Ho:YAG laser (macropulse of 300 μs consisting of microsecond micropulses) used in this study and in the clinic. Third, in the previous study a lens was used to focus the laser beam onto the stone sample, while in this study an optical fiber with diverging output beam was used in a similar method as in the clinic. Fourth, in the previous study, COM stones were cut with a diamond saw to produce a flat surface and then irradiated in a dry environment, while in this study COM stones with rough surfaces in their natural hydrated state were irradiated, again similar to in the clinic.

The difference between the ablation thresholds of the Ho:YAG and TFL for a given stone type may be due in part to the difference in water absorption coefficients at the two wavelengths (μ_a = 28 vs. 160 cm^{-1}) [15] for the bound water component of the stone as well as the surrounding hydrated environment in the urinary tract. Otherwise, the absorption curve for dehydrated human COM stones in the near-infrared from 1500-

2000 nm is relatively flat and independent of wavelength [21], so the hard tissue component of the stone probably does not significantly contribute to the large difference in absorption coefficients for COM stones at the two wavelengths.

The TFL is able to ablate stones with four times less energy than the Ho:YAG laser. This allows TFL operation at a much lower laser pulse energy than would be needed for the Ho:YAG during lithotripsy. Using less energy should also translate into less stone retropulsion [22-23]. Furthermore, the ability of the TFL to operate at higher pulse rates may even increase ablation rates while minimizing retropulsion.

2.3.2 Ablation Rates

The Ho:YAG ablation rate increased linearly with pulse energy for COM stones (Figure 10) and UA stones (Figure 11), resulting in a COM stone vaporization rate of 100 µg/s at a pulse energy of about 165 mJ and about 37 µg/s at 35 mJ. Because of the ease at which UA stones are fragmented using high pulse energies, energy studies beyond 35 mJ using the Ho:YAG were not comparable since vaporization was no longer a dominant form of ablation.

On the contrary, although the TFL ablation rate also continued to increase with increasing pulse rate, the rate of increase did not appear linear, as shown in Figure 12 for COM stones and Figure 13 for UA stones. Instead, an increase in pulse rate from 10 to 100 Hz did not result in an anticipated ablation rate increase of 10-fold, but rather only a 5-fold increase from 28 to 140 µg/s for COM stones and a 7-fold increase from 48 to 335 µg/s for UA stones.

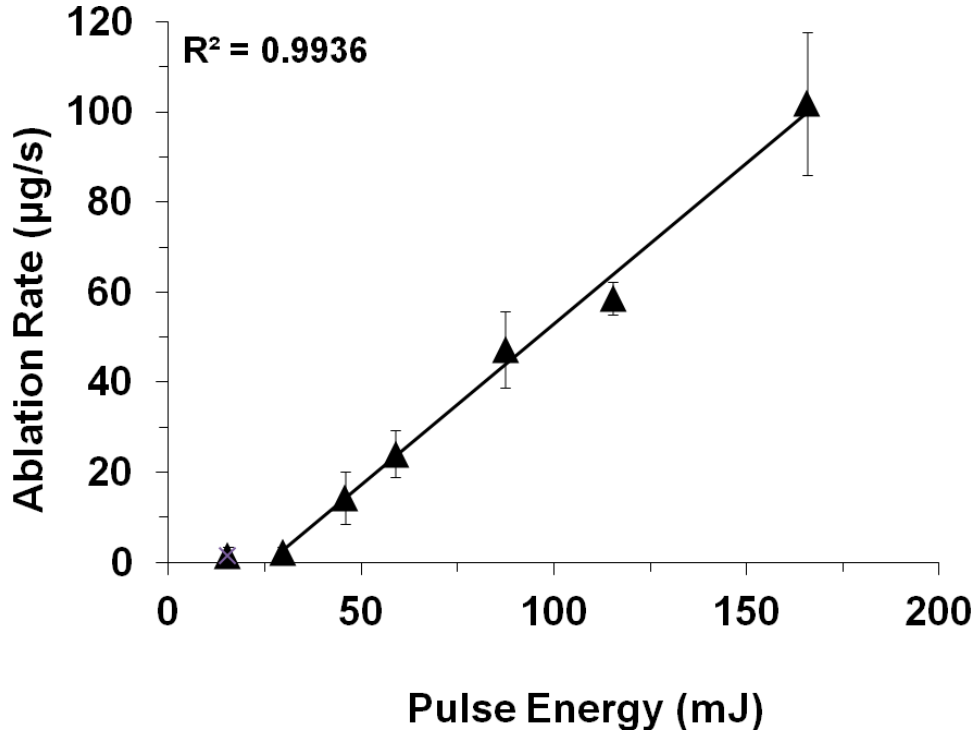

Figure 10. Ablation rates of COM stones using Ho:YAG with increasing pulse energy at a fixed pulse rate of 10 Hz.

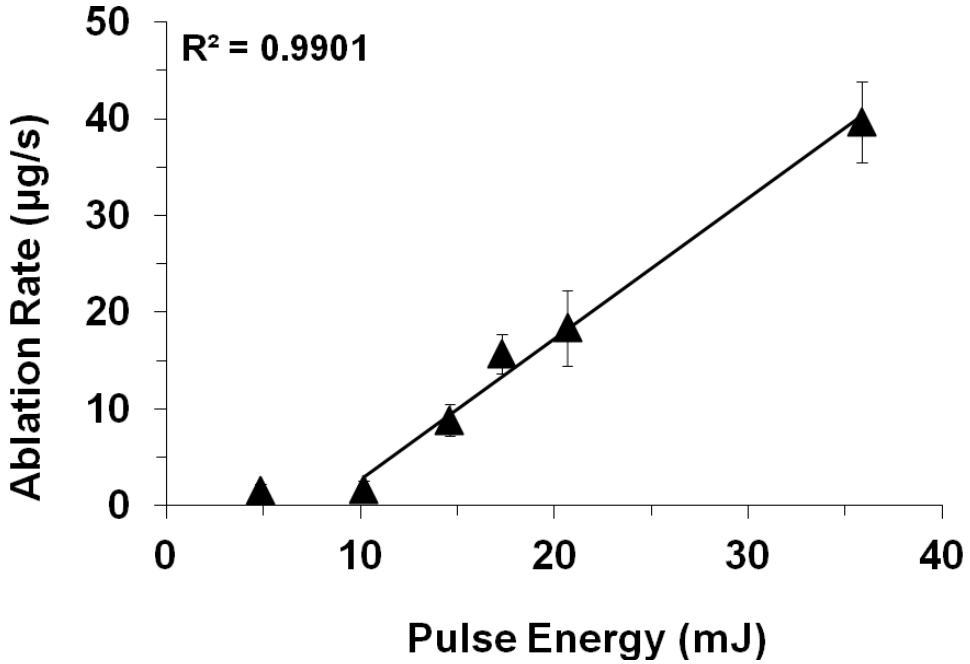

Figure 11. Ablation rates of UA stones using Ho:YAG with increasing pulse energy at a fixed pulse rate of 10 Hz.

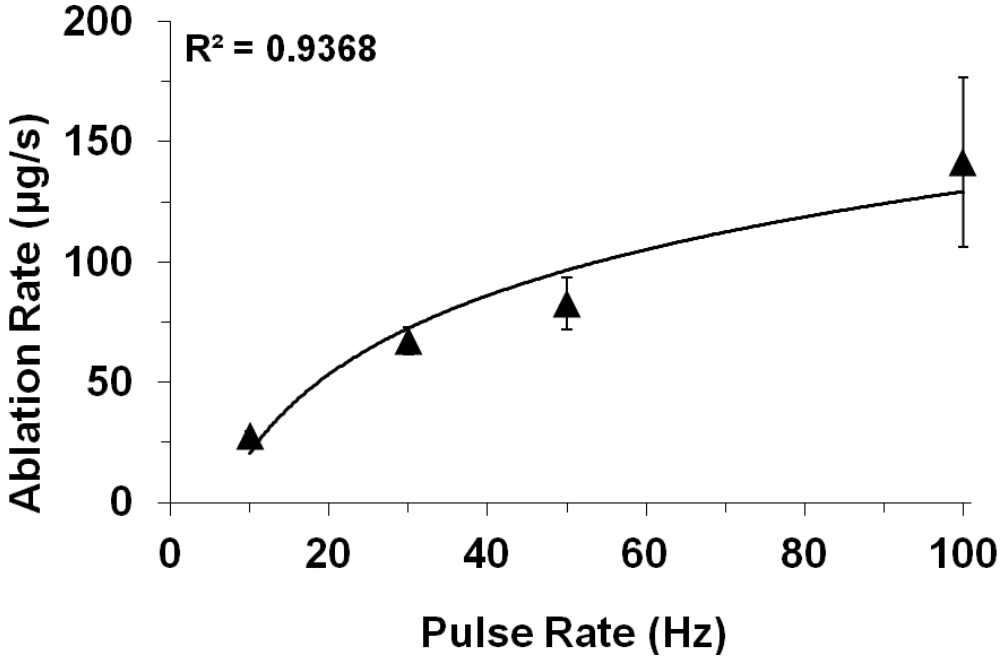

Figure 12. Ablation rates of COM stones using TFL with increasing pulse rates at a fixed pulse energy of 35 mJ.

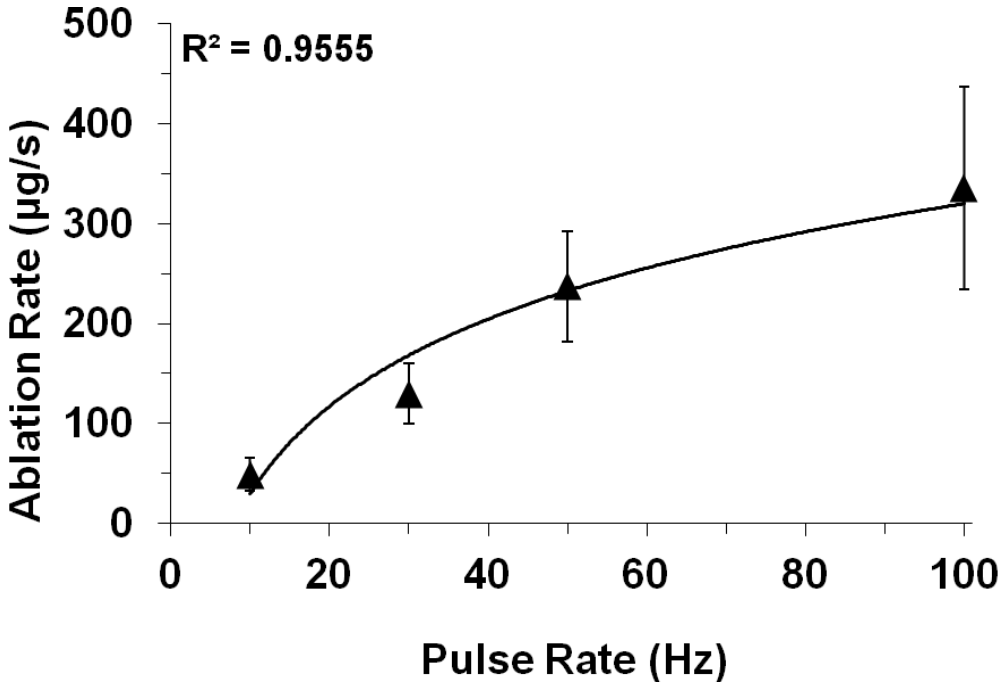

Figure 13. Ablation rates of UA stones using TFL with increasing pulse rates at a fixed pulse energy of 35 mJ.

It is possible that some of the stone ablation efficiency lost during operation at high pulse rates was due to absorption of a higher fraction of laser pulses in the saline bath as the fiber was scanned across the stone surface, although this contribution requires further study. Charring of the stone surface was also observed at TFL pulse rates above 100 Hz, most likely as a result of thermal buildup as the stone was kept fixed during the study. However, in a clinical environment involving stone mobility, regular saline irrigation, and cooling of the stone surface, efficient TFL operation at pulse rates higher than 100 Hz may be feasible (if stone retropulsion is not a concern) and warrants further study. Nevertheless, operation of the TFL at higher pulse rates still results in an increase in the ablation rate, and at relatively little expense, since the diode-pumped fiber laser is capable of operating at arbitrary pulse rates from 1-1000 Hz.

Although the laser pulse energies used in this study are still significantly lower than the minimum pulse energies typically used in the clinic (400-600 mJ/pulse), it should be noted that the Ho:YAG laser pulse energy cannot be increased indefinitely because of stone retropulsion. As mentioned before, although commercial Ho:YAG lasers are available with pulse rates up to 50 Hz (e.g. for treatment of BPH), these systems are quite large and expensive, and actually consist of four Ho:YAG laser heads packaged into one system. This design is necessary because thermal effects occur in the laser rod of a flashlamp-pumped, solid-state Ho:YAG laser system, which typically leads to a significant decrease in pulse energy as the pulse rate is increased beyond 10 Hz as shown in Figure 14 [6].

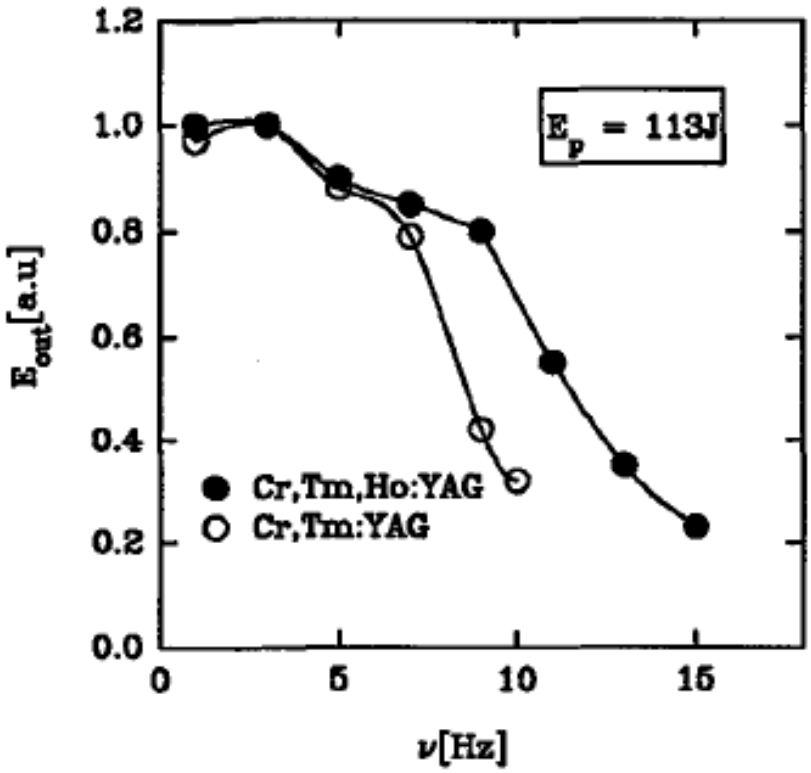

Figure 14. Decrease of energy output as the pulse rate is increased for the Ho:YAG and other lasers [6].

2.4 Conclusion

The ablation threshold for both stones, COM and UA, was four times lower using the TFL than with the Ho:YAG. The COM stone ablation threshold for the Ho:YAG and TFL measured 82.6 J/cm^2 and 20.8 J/cm^2, respectively. The UA stone ablation threshold for Ho:YAG and TFL measured 25.9 J/cm^2 and 6.5 J/cm^2 respectively. An increase in ablation rates is seen with increasing pulse energy using the Ho:YAG and increasing pulse rates using the TFL, but the cost of this increase with the Ho:YAG is a potential increase in retropulsion. The use of lower energy using the TFL to achieve better

ablation rates than the conventional Ho:YAG is a promising achievement in the development of TFL lithotripsy treatment of urinary stones.

CHAPTER 3: STONE RETROPULSION

3.1 Introduction

Retropulsion is defined as the movement of a stone due to laser irradiation. Clinicians use x-ray fluoroscopy and flexible endoscopes incorporating magnifying optics to navigate through the urinary tract and locate stones. Once the stones are located, the clinician presses the fiber tip to the stone and delivers a train of laser pulses. Figure 15 shows the various locations of a stone within the urinary tract. If the pulse energy is sufficiently large to push the stone, the stone will migrate from the ureter to a calyx in the kidney. The clinician may then waste considerable time tracking down the new location of the stone. Therefore, it is ideal to minimize retropulsion of urinary stones during lithotripsy.

Retropulsion is caused by forces acting on the stone. Three sources have been explored to determine the cause of retropulsion. The most obvious force, resulting from radiation pressure, is negligible when considering forces resulting from pressure waves. For instance, the largest radiation pressure our lab is able to produce (using a 100 Watt CW laser with a 100-μm-core fiber) is orders of magnitude less than reports of mechanical forces measured with a hydrophone [24-26]. Two other theories are discussed below.

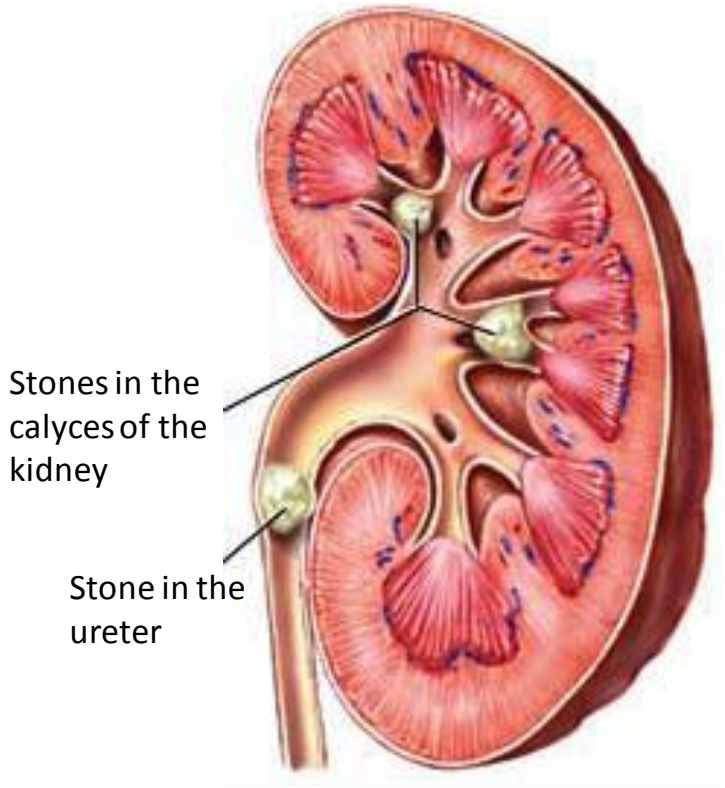

Figure 15. Diagram of stone locations within the kidney (adapted from [27]).

One theory states that retropulsion is due to a combination of mechanical forces exerted against the stone by the ejected fragments [28]. When a crater is created in the stone, the only direction for the fragments to go is in the opposite direction of the stone. If a larger fiber is used, a more shallow and wide crater is formed. This leads to more of the fragments being ejected in the direction opposite of energy delivery. But, when a smaller fiber is used, a deeper and narrower crater is formed. This leads to the forces in the radial x-direction being greater, cancelling each other out, and leaving a smaller net force in the axial y-direction. Figure 16 illustrates the direction of forces from particle ejection during the creation of stone craters. When the addition of forces of ejected particles on the stone is considered, a deep and narrow crater is more desired so that the

forces in the y-direction are smallest ($Y_A<Y_B$). This suggests the use of smaller fibers is better suited to reduce retropulsion.

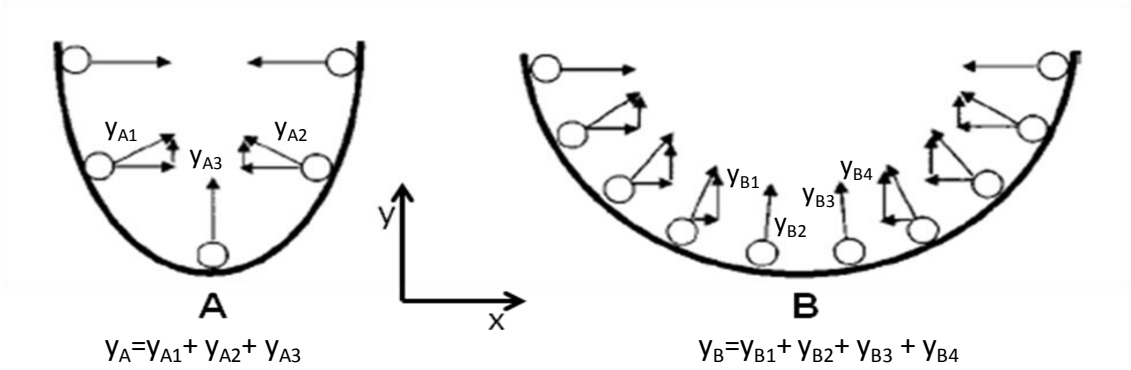

Figure 16. A) Crater formed from irradiation through a narrow fiber. B) Crater formed from irradiation through a wide fiber (adapted from [28]).

Another theory states that the shockwave induced from the rapid expansion and collapse of cavitation bubbles is responsible for retropulsion [7, 9-11]. The sequence of the expansion and collapse of a cavitation bubble induced by the Ho:YAG laser is shown in Figure 17. When water is irradiated with infrared energy, the light is quickly absorbed and forms a vapor bubble. This bubble expands and collapses rapidly. The rapid expansion and collapse creates pressure waves in the surrounding medium. Shorter pulses result in quicker expansion and collapse of cavitation bubbles, contributing to an increase in the intensity of the pressure wave. Pressure waves can be used to fragment urinary stones, but the waves created by long-pulsed, infrared radiation have been shown not to correlate with stone ablation [29-34]. They can, however, cause the urinary stone to bounce away from the fiber tip, resulting in retropulsion.

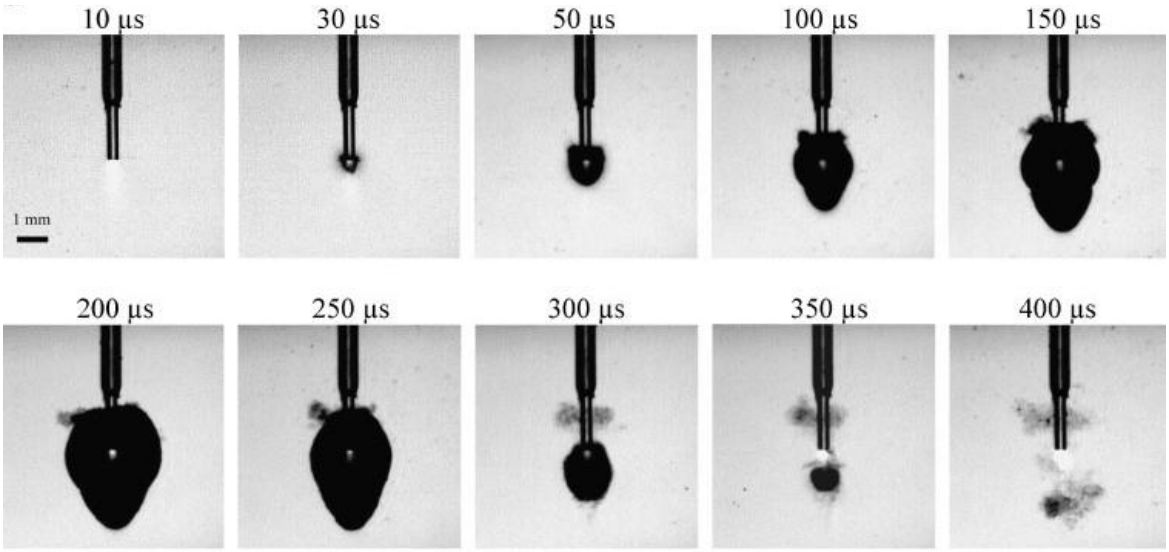

Figure 17. Cavitation bubble expansion and collapse using a Ho:YAG with a pulse duration of 150 µs (FWHM) using a 365 µm fiber and 800 mJ pulse energy [11].

3.2 Methods

A clinical Holmium:YAG laser (TwoPointOne XE, Coherent, Santa Clara, CA) was operated with a wavelength of 2120 nm, variable pulse energies of 30-540 mJ, 300-µs pulse duration, and a pulse rate of 10 Hz. For comparison, an experimental TFL (TLR 110-1908, IPG Photonics, inc., Oxford, MA) was externally modulated with a function generator (Model DS345, Stanford Research Systems, Sunnyvale, CA) to operate in pulsed mode with a wavelength of 1908 nm, pulse energies of 35 mJ, 500-µs pulse duration, and pulse rates ranging from 10-400 Hz.

Spherical Plaster-of-Paris (PoP) stone phantoms having approximately the same size (6-mm-diameter) and density as COM stones were created using a mold, and then used for the stone retropulsion studies as a standard model for providing more reproducible results than the irregularly shaped COM stones. A minimum of five stone

samples were used for each set of laser parameters and the mean ± standard deviation was plotted for each data point.

Laser energy was delivered through 270-µm optical fibers (Olympus Gyrus ACMI, Southborough, MA) in contact mode with 6-mm-diameter (PoP) stone phantoms, submerged in a saline bath (Figure 18). A rigid ureteroscope (9.5-Fr ID, Karl Storz, Germany) attached to a light source (X7000, Stryker Endoscopy, San Jose, CA), camera (1188HD, Stryker), and monitor, was used to accurately position the optical fiber tip so it was perpendicular to, centered on, and in contact with the PoP stone phantom prior to irradiation. Stone retropulsion distance was measured for each set of laser parameters, for a fixed total energy (42 J) delivered to the stone.

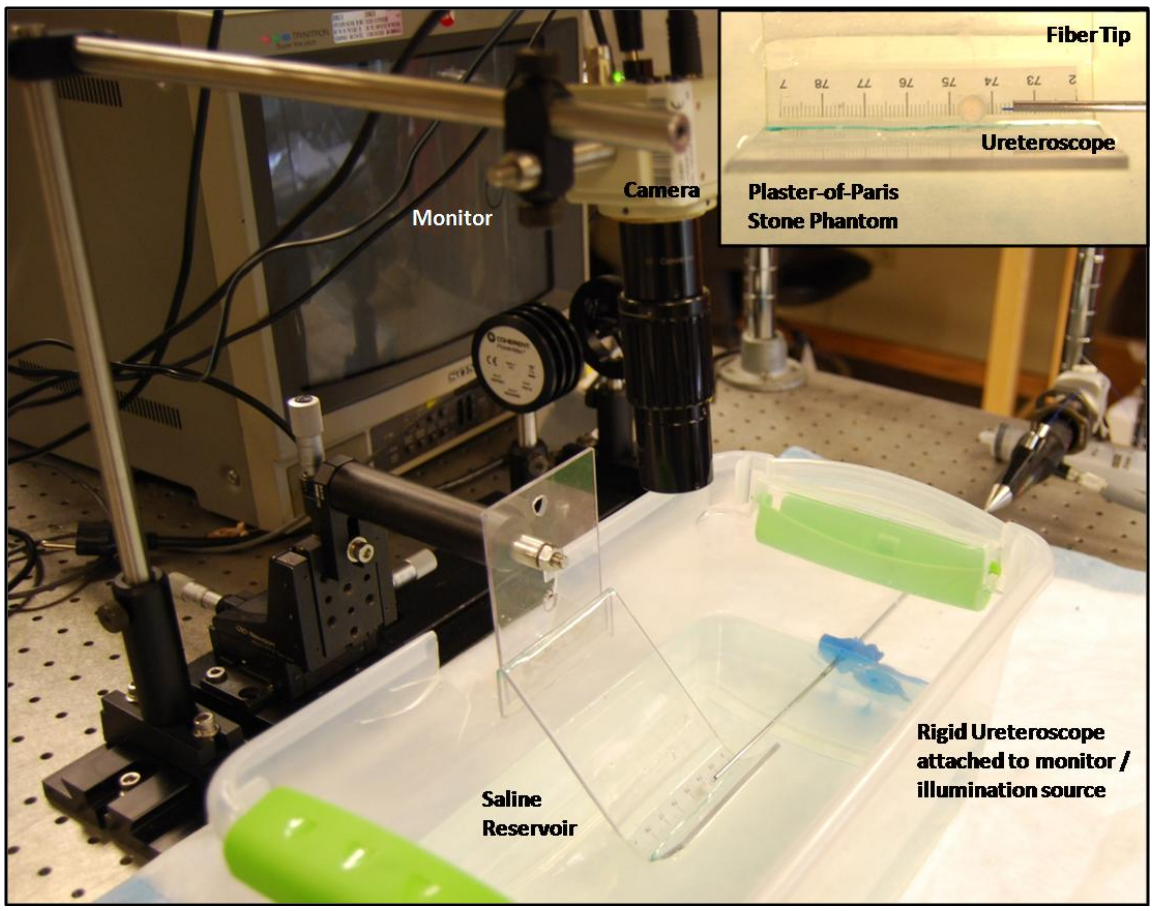

Figure 18. Experimental setup for studying retropulsion during Holmium:YAG and Thulium fiber laser lithotripsy using plaster-of-Paris stone phantoms. A rigid ureteroscope attached to a light source, camera, and monitor, was used to accurately position the optical fiber tip so it was perpendicular to, centered on, and in contact with the stone prior to irradiation.

3.3 Results

Retropulsion with the Ho:YAG laser seemed to increased linearly with increasing pulse energy (Figure 19). Retropulsion with the TFL was minimal at pulse rates less than ~ 150 Hz, then rapidly increased with higher pulse rates (Figure 20). For a direct comparison, retropulsion is shown for both lasers as a function of power (Figure 21). For the purposes of this study, minimal retropulsion was defined as a retropulsion distance of less than 2 mm. This criteria would imply that Ho:YAG laser settings of greater than 175

mJ at 10 Hz with a 270-µm fiber results in significant retropulsion. TFL lithotripsy at pulse rates greater than 150 Hz at 35 mJ resulted in significant retropulsion as well.

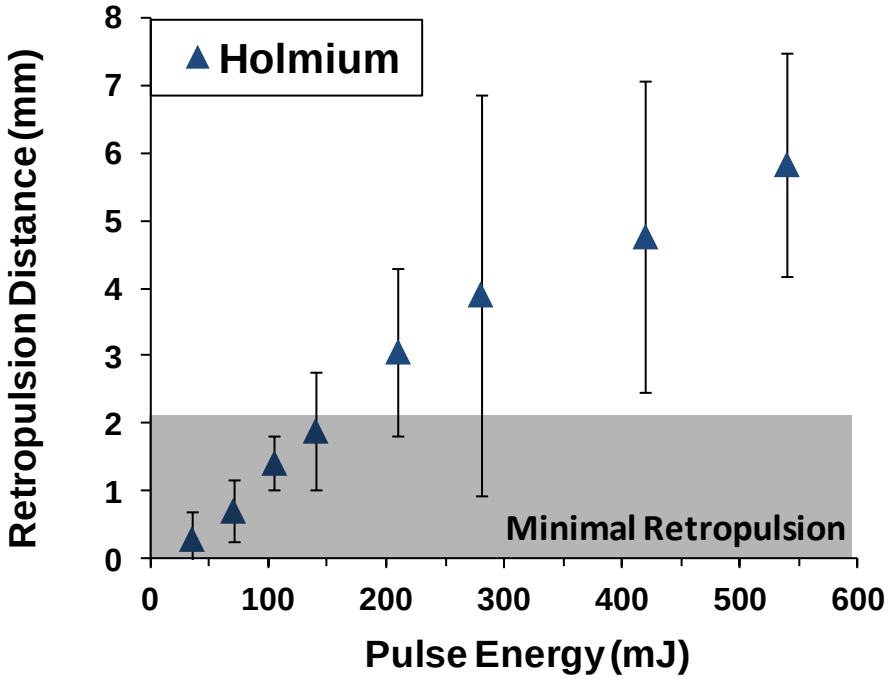

Figure 19. Retropulsion distance for 6-mm-diameter plaster-of-Paris stone phantoms as a function of pulse energy for Ho:YAG laser operated at a fixed pulse rate of 10 Hz**.**

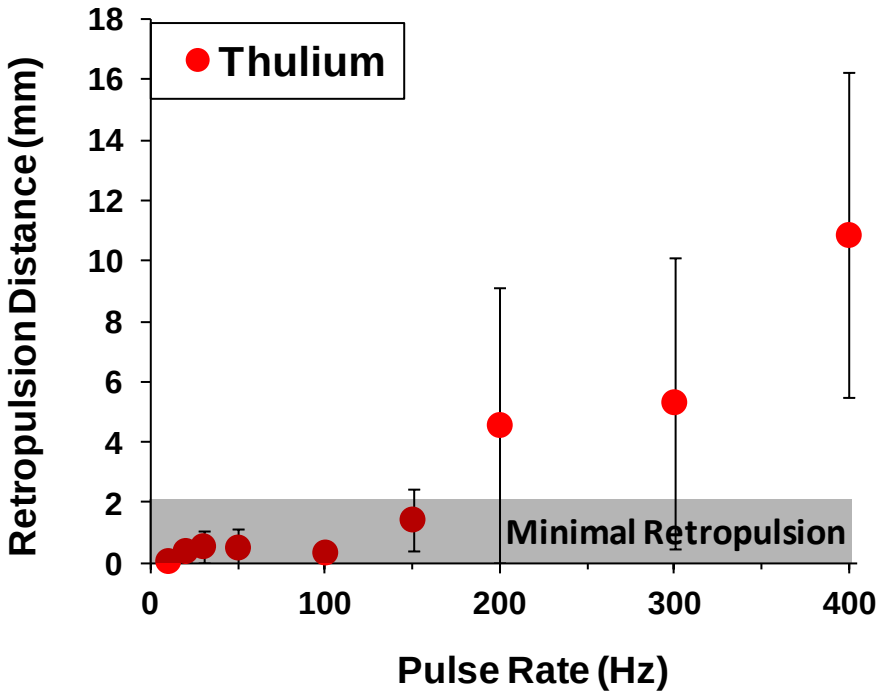

Figure 20. Retropulsion distance for 6-mm-diameter plaster-of-Paris stone phantoms as a function of pulse rate for TFL operated with a fixed pulse energy of 35 mJ.

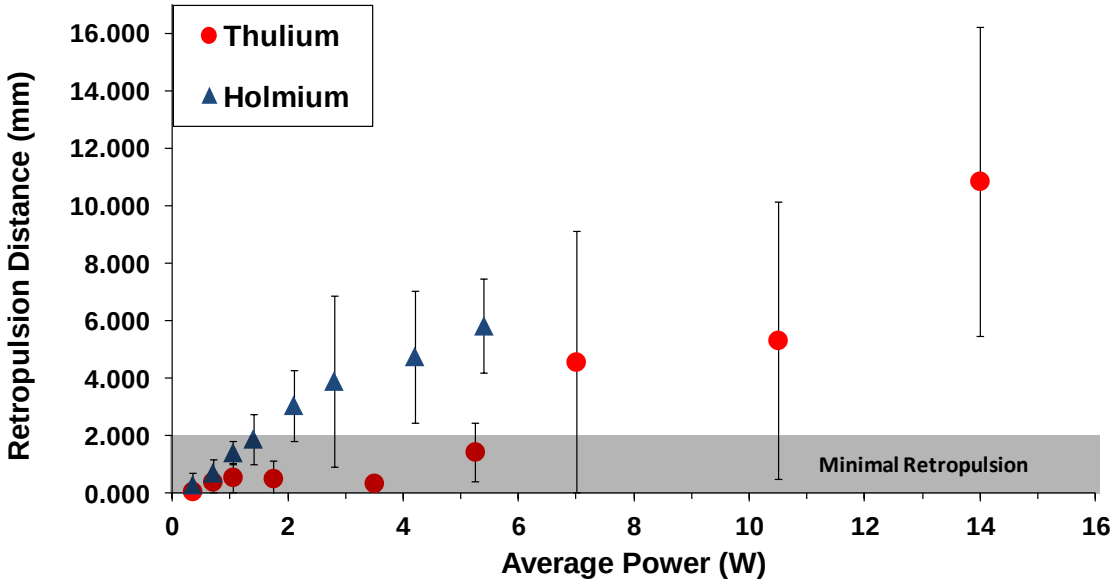

Figure 21. Retropulsion distance for 6-mm-diameter plaster-of-Paris stone phantoms as a function of power for the TFL with fixed pulse energy of 35 mJ and varying pulse rate and Ho:YAG with a fixed pulse rate of 10 Hz and varying pulse energy.

3.4 Discussion

Retropulsion with the Ho:YAG laser seemed to increased linearly with increasing pulse energy. Retropulsion with the TFL was minimal at pulse rates less than 150 Hz, then rapidly increased with higher pulse rates. The amount of stone retropulsion that would be considered acceptable in a clinical study is not easy to quantify. However, for the purposes of this study, minimal retropulsion was defined to be a retropulsion distance of less than 2 mm. This value is based in part on the observation that the fiber tip to stone surface working distance needs to be short, providing near-contact working conditions, for efficient stone vaporization during Ho:YAG lithotripsy. This criteria would imply that Ho:YAG laser settings of greater than 175 mJ with a 270-µm fiber results in significant retropulsion. This energy level is considerably less than the lowest settings of 400-600 mJ typically available with a clinical Ho:YAG laser system. Indeed, this study confirms what urologists already experience in the clinic, a significant retropulsion effect that results in the clinician having to waste time "chasing" stone fragments inside the urological tract. TFL settings of greater than 150 Hz resulted in significant retropulsion as well.

In summary, if both the ablation rate and retropulsion experimental data are considered in unison rather than as separate studies, the results would indicate that a Ho:YAG pulse energy of 165 mJ (at 10 Hz) capable of minimizing stone retropulsion results in an ablation rate of 100 µg/s. A TFL pulse rate of 100 Hz (at 35 mJ), capable of minimizing stone retropulsion, results in an ablation rate of 140 µg/s. Furthermore, the TFL is able to deliver up to 4.5 times more power than the Ho:YAG to the stone without causing significant retropulsion. Thus, if the urologist is concerned about minimizing

stone retropulsion effects at the expense of lower stone ablation rates, then the TFL may represent a viable alternative to the Ho:YAG laser. Previous studies reporting on the optimal set of Ho:YAG laser parameters for efficient lithotripsy with minimal stone retropulsion have reached similar conclusions that operation of the Ho:YAG laser with lower pulse energies and higher pulse rates than typically used in the clinic would also be beneficial [22-23].

Furthermore, recent Ho:YAG laser lithotripsy retropulsion studies have concluded that the use of lower pulse energies, longer pulse durations, higher pulse rates, and smaller optical fiber diameters is the optimal combination of laser parameters for minimizing stone retropulsion [7-12]. A comprehensive study of all of these parameters was beyond the scope of this experiment. It may also be necessary to calculate the forces working on the stone to determine optimal parameters to limit retropulsion. However, it should be emphasized that, unlike the flashlamp-pumped Ho:YAG laser, the diode-pumped TFL is an ideal laser for operation within the range of laser parameters listed above, due to the TFL's excellent spatial beam profile which allows use of small-core fiber diameters and its operation at arbitrary pulse durations and pulse rates.

3.5 Conclusion

Stone retropulsion with the Ho:YAG laser increased linearly with pulse energy. Retropulsion with the TFL was minimal at pulse rates less than 150 Hz, then rapidly increased at higher pulse rates. Retropulsion with the Ho:YAG laser was minimal for pulse energies less than 175 mJ. Combining these results with the findings in Chapter 2, the TFL provided comparable ablation rates to the Ho:YAG laser for pulse energies and

pulse rates that lead to minimal retropulsion. These results are another positive indication that the TFL is a viable alternative to the conventional Ho:YAG laser.

CHAPTER 4: TAPERED FIBERS FOR TFL LITHOTRIPSY

4.1 Introduction

Several problems are associated with using optical fibers inside flexible endoscopes. Tight bending diameters of 1 cm or less are necessary to reach urinary stones in the lower pole of the kidney. The endoscopes are sufficient to satisfy such extreme bending conditions. However, when a fiber is present in the working port of the endoscope, it may hinder endoscope deflection, or even break. Should the fiber break or not be pushed completely through, perforation of these expensive endoscopes may occur if the laser is firing [35-36].

Medical fiber optic companies have attempted numerous approaches to reducing fiber failure on the fiber input end during coupling of high-power Ho:YAG laser power into connectorized small-core fibers [13, 37]. These approaches include ferrule designs which absorb or direct excess energy away from the fiber cladding. These designs result in wasteful losses of laser power and inefficient fiber coupling, and the need for a higher power and more expensive laser system. Tapered tip designs have also been used at the fiber input end to couple the beam. These fibers typically result in the creation of higher order modes which can escape into the fiber cladding, creating an even poorer spatial beam profile at the fiber output end. Ho:YAG lasers also produce high amounts of heat, causing “thermal lensing.” Thermal lensing is occurs when heating of the laser rod

causes mechanical changes of the rod and changes in the refractive index. This changes the intensity distribution of the laser spatial beam profile, and potentially leads to misalignment of the laser beam with the fiber input end, thus resulting in fiber damage [38].

The ideal optical fiber for use in laser lithotripsy would have several important properties: (1) biocompatibility, (2) flexibility for use in ureteroscopes in the upper urinary tract, (3) small diameter providing space for high saline irrigation rates through the ureteroscope and increased visibility, (4) high optical damage threshold to provide transmission of high laser powers, and (5) a large tip diameter to provide robust mechanical and chemical properties and minimize pitting, fracture, and burn-back of the fiber tip during lithotripsy.

Unfortunately, conventional optical fibers do not satisfy all of these criteria in a single design (Table 1). Smaller optical fiber diameters provide the benefit of increased flexibility and irrigation rates. However, these smaller diameter tips are more fragile and likely to mechanically degrade and suffer from “burn-back” more rapidly than larger diameter fibers [39]. Larger diameter optical fibers transmit higher laser power and are more robust. However, larger fibers are also less flexible and use more space in the working port of an endoscope, thus reducing irrigation rates and visibility during lithotripsy.

Table 1. Comparison of small versus large core optical fibers for use in laser lithotripsy

Properties	Small-Core	Large-Core
Flexibility	+	-
Irrigation	+	-
Power delivery	-	+
Durability	-	+

While tapered fibers are commercially available and are routinely used for laser lithotripsy [40] and laser surgery in general, they are usually available in one of two configurations: either with a short taper on the input fiber end to allow coupling of the large, multimode Ho:YAG laser beam into the fiber at high powers, or as a gradual taper along the entire fiber length. Neither of these designs satisfies the criteria listed above for an ideal lithotripsy fiber.

The objective of this preliminary study is to describe a TFL and tapered optical fiber delivery system combination that may provide many of the advantages described above without many of the limitations. We evaluate the performance of this tapered fiber system and compare it with conventional laser lithotripsy fibers.

A tapered fiber consists of a funnel-shaped core (Figure 22a) [41]. Normally, this fiber is used in a large-to-small diameter configuration to couple a large laser beam into the proximal end of the fiber, and then reduce the fiber diameter for additional flexibility. However, the advantage of more easily coupling the laser beam into the proximal fiber end may be partially offset by the disadvantage of the beam being more highly diverging at the distal fiber end. This configuration results in the creation of higher order modes

which can escape into the fiber cladding, increasing the probability of fiber damage and creating an even poorer spatial beam profile at the fiber output end [37].

However, the use of the TFL for lithotripsy provides a unique opportunity to reverse the orientation of the tapered fiber, and instead use the taper on the distal fiber tip in a small-to-large diameter configuration (Figure 22b). This alternative tapered configuration is possible because the excellent spatial beam profile of the TFL provides easy coupling of high laser powers into the proximal end of small-core fibers without risk of damage to the fiber [42]. Thus, in theory, the distal tapered fiber tip may provide several advantages: (1) less divergence of the output beam, (2) a larger diameter and more robust fiber tip less likely to be damaged or experience burn-back when in contact with the stone, and (3) a larger cross-sectional treatment area on the stone.

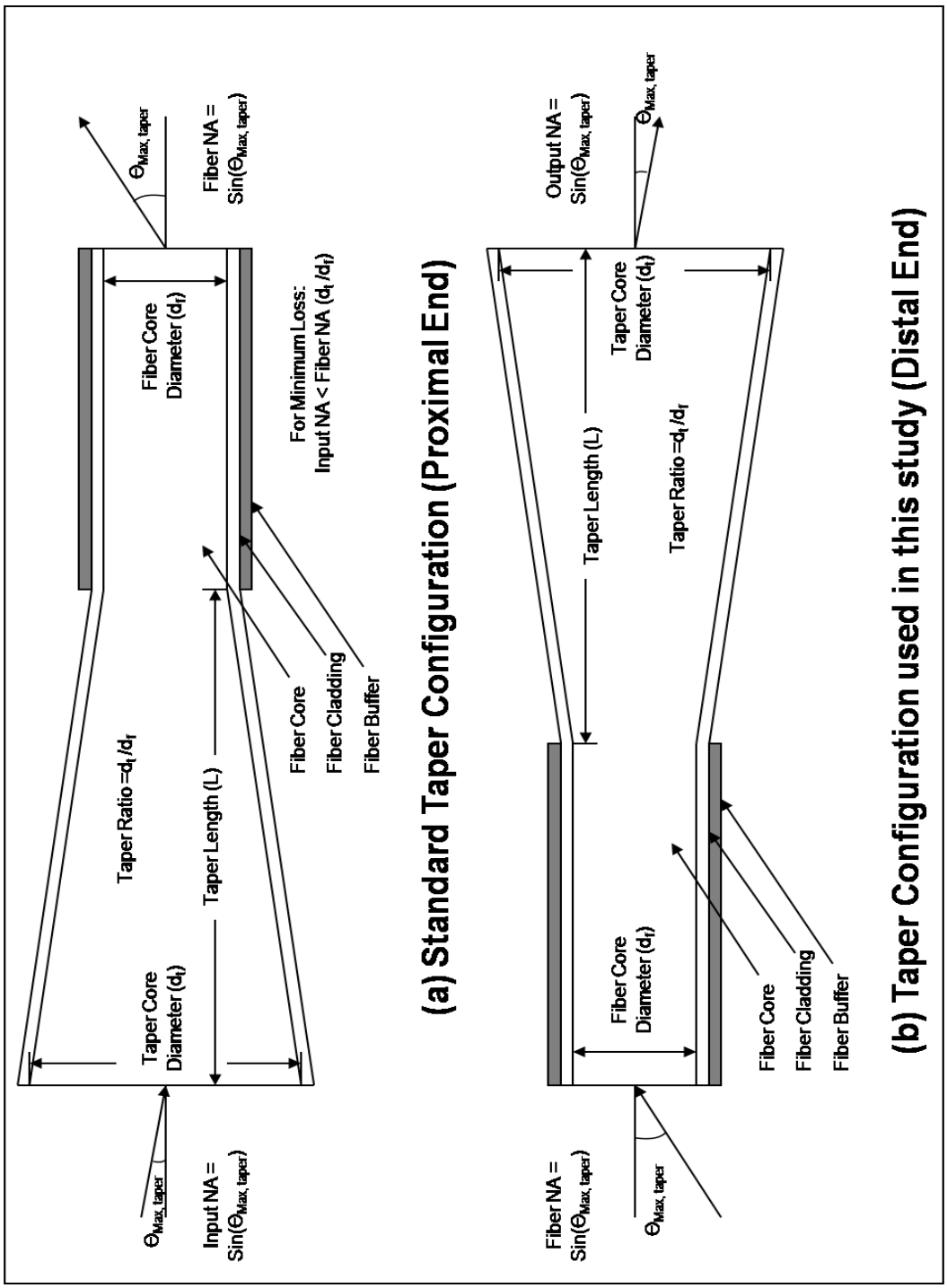

Figure 22. Geometry of the tapered fiber. (a) Standard configuration where taper is used on the proximal end of the fiber; (b) Configuration used in this study where taper is used on the distal end of the fiber. Figure adapted from [41].

4.2 Materials and Methods

A 100-Watt TFL (Model TLR 110-1908, IPG Photonics, inc., Oxford, MA) with a center wavelength of 1908 nm was used in these studies. The laser was electronically modulated with a function generator (DS345, Stanford Research Systems, Sunnyvale, CA) to produce 1-ms pulses, and operated at a pulse rate of 10 Hz for lithotripsy studies. A 50-mm-FL calcium fluoride lens was used to focus the 5.5-mm-diameter collimated fiber laser beam down to a spot diameter of approximately 75 µm ($1/e^2$), for coupling into the small-core optical fibers. The fiber output pulse energy was kept fixed at 70 mJ for these studies.

Figure 23 shows the tapered fiber that was used in these studies (150-µm-core to 300-µm-core taper over a 5-mm-length at the distal tip (FIPE150165195, Polymicro, Phoenix, AZ). Several different small-to-medium sized conventional fibers were compared to the tapered fiber in various experiments: 100-µm, 200-µm, 270-µm, and 365-µm-core fibers (Thorlabs, Newton, NJ); 150-µm and 300-µm-core fibers (Polymicro, Phoenix, AR); 270-µm-core fiber (Olympus Gyrus ACMI, Southborough, MA). All of these fibers consisted of conventional low-OH silica cores, but differed in their cladding and jacket materials and outer diameters.

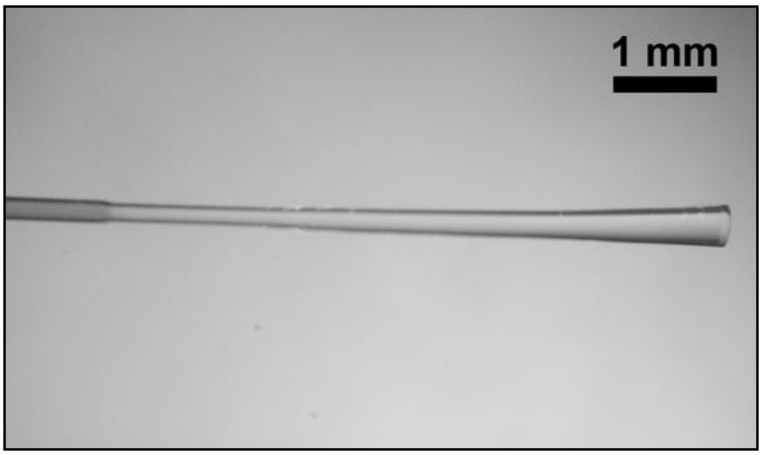

Figure 23. Image of the tapered fiber used in this study, which consists of a 150-µm-core-diameter trunk fiber, with a distal fiber tip expanded to a 300-µm-core-diameter over a 5-mm length.

Human UA and COM urinary stone samples were used for this study. The initial stone mass was recorded with an analytical balance (AB54-S, Mettler-Toledo, Switzerland) before securing the stone in place with a clamp. The clamp and the stone were then submerged in a saline bath. The laser radiation was delivered through the handheld fiber to the stone surface in a scanning motion to provide uniform vaporization, as in Chapter 2. After delivery of 1800 pulses, the stone was then removed from the saline bath and allowed to completely dry before the final mass was recorded. Ten samples were tested for each data set for the lithotripsy studies, and the mean $\pm$ standard deviation (S.D.) was recorded. A paired student's t-test was performed to determine statistical significance ($P < 0.05$) between fiber data sets (conventional vs. tapered fibers) for both UA and COM stone types.

A time-domain endoscopic optical coherence tomography (OCT) system (Niris, Imalux, Cleveland, OH) was used with an 8 Fr (2.6-mm-OD) probe to image cross-sectional depths of the ablation craters for the tapered fiber. The axial resolution was

approximately 11 µm and the lateral resolution was approximately 25 µm. The lateral scanning distance was 2 mm and the imaging depth was 1.6 mm. The OCT probe was placed at normal incidence in near-contact with the ablation crater on the stone surface for image acquisition. The effect of fiber-to-stone working distance on stone vaporization was also observed using OCT. The tapered fiber tip was placed at different distances from the stone surface in a saline environment, and the ablation crater was imaged after 10 pulses delivered at 70 mJ, 1 ms, and 10 Hz.

Fiber transmission loss and fiber length loss ("burn-back") were measured for both 150/300 µm tapered fibers and conventional 150 µm fiber tips in contact with human UA and COM stones for the same laser parameters (70 mJ, 1 ms, 10 Hz, and 1800 pulses). Transmission losses were determined using a power meter (EPM 2000, Coherent, Santa Clara, CA) by measuring the average power before and after the procedure. The pulse energy was then calculated by dividing the average power by the pulse rate. The fiber tip was consistently maintained at a fixed distance from the detector (PM100-19C, Coherent) for each measurement. Fiber burn-back was quantified by measuring the distance of the exposed distal fiber tip from the jacketed fiber both before and after the procedure. The difference between these two measurements was defined as the fiber burn-back. A total of 20 stones (10 UA and 10 COM) were used for this study.

Saline irrigation rates through the 3.6 French (1.2 mm) inner diameter working port of a flexible ureteroscope (Invisio DUR-D, Olympus Gyrus ACMI, Southborough, MA) were measured for different type and size fibers ranging from 100-400 µm-core-diameter. A saline bag elevated 100 cm above the endoscope was used for gravitational flow measurements, and the amount of saline filling a beaker after 2 min of flow was

recorded (n = 3 measurements for each fiber size). The irrigation rate (ml/min) was measured and compared to the rate without fiber. A percent (%) flow was then recorded by dividing the flow rate with fiber in the working port by the flow rate without fiber in the working port.

Ureteroscope bending tests were also performed to determine the maximum primary and secondary angles of deflection of the ureteroscope as a function of the fiber diameter inserted through the working port. The same ureteroscope and fiber diameters as used during the irrigation rate studies were also used in this study. The fibers were inserted through the working port of the ureteroscope tip, as shown in Figure 24, which was then photocopied at its maximum angle of deflection. A protractor was used to measure the angle of deflection using a method previously reported [43].

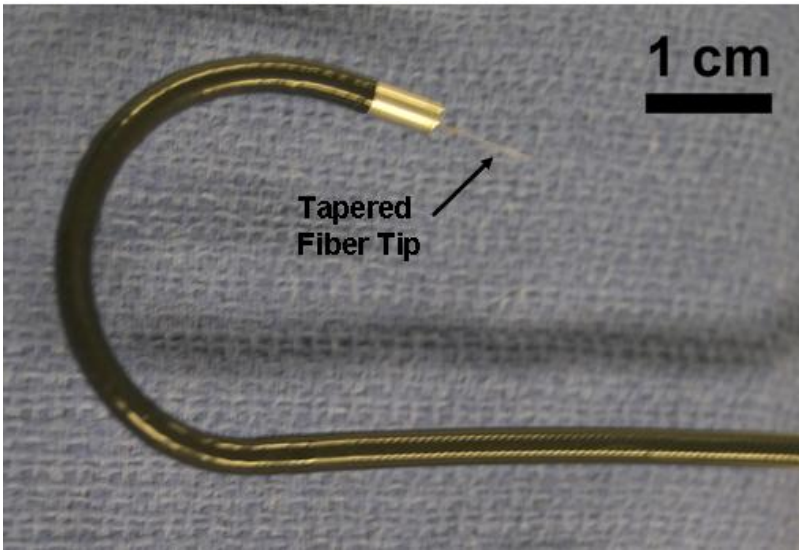

Figure 24. Deflection of ureteroscope with the inclusion of a tapered fiber.

4.3 Results

Five experimental studies were conducted to characterize the tapered fiber tips during TFL lithotripsy: (1) Comparison of mass loss after stone vaporization between 150/300 µm tapered fibers and conventional 100-µm fibers; (2) Effect of fiber tip to stone working distance on ablation efficiency for the 150/300 µm tapered fibers; (3) Comparison of optical (transmission losses) and mechanical properties (fiber burn-back) for 150/300 µm tapered fibers and conventional 150-µm fibers; (4) Measurement of irrigation rates through an ureteroscope during insertion of a 150/300 µm tapered fiber; and (5) Measurement of the maximum primary and secondary angles of deflection of the ureteroscope during insertion of a 150/300 µm tapered fiber.

For the stone vaporization studies, stone mass removed for each fiber for the same total number of laser pulses (1800) and total energy (126 J) delivered to the stone was measured (Table 2). There was no significant difference in the mass loss between fibers for a given stone type, demonstrating that the tapered fiber provides comparable mass loss and vaporization rates to that of a conventional small-core fiber.

Table 2. Stone mass loss as a function of fiber type and stone composition

Fiber	150/300 µm Taper	100 µm Standard	n
Stone Type			
UA*	12.7 $\pm$ 2.6 mg	12.6 $\pm$ 2.5 mg	10
COM*	7.2 $\pm$ 0.8 mg	6.8 $\pm$ 1.7 mg	10

* $P > 0.05$: no significant difference between fibers for a given stone type.

Figure 25 shows ablation craters at different working distances of 0, 500, and 1000 µm. TFL vaporization of the stone was observed to "stall out" for distances greater than about 1 mm, due to intervening water absorption. This study demonstrates that TFL lithotripsy through a tapered fiber is feasible in contact and near-contact mode, as the theoretical model would suggest (Figure 22).

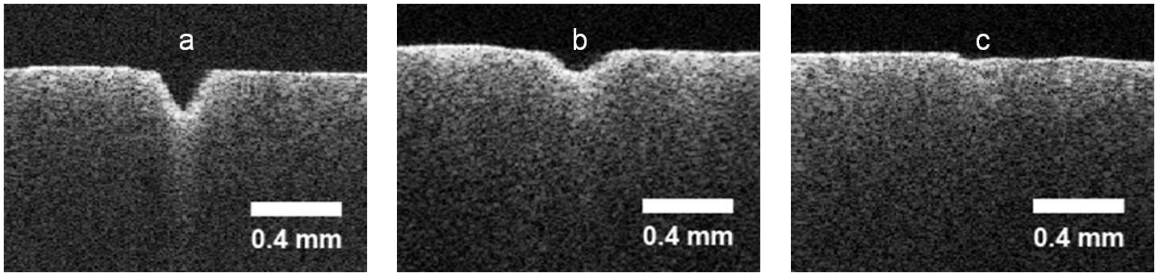

Figure 25. Effect of fiber-to-stone working distance on stone vaporization measured using optical coherence tomography at different working distances in a saline environment; (a) Working distance of 0 µm (contact mode); (b) Working distance of 500 µm; (c) Working distance of 1000 µm. TFL vaporization of the stone completely "stalls out" due to intervening water absorption, for working distances greater than approximately 1 mm, for the laser parameters used in this study.

Another study was conducted to test the optical and mechanical durability of the tapered fiber tip during laser lithotripsy. Fiber transmission loss and fiber length loss ("burn-back") were measured for both 150/300 µm tapered fibers and conventional 150 µm fiber tips in contact with human UA and COM stones for the same laser parameters (70 mJ, 1 ms, 10 Hz, and 1800 pulses). The results of this study are provided in Table 3. There was no evidence of transmission loss or burn-back for the tapered fiber after treating a total of 20 stone samples, including both UA and COM stones (1800 pulses/stone x 20 stones = 36,000 pulses). On the contrary, the conventional 150 µm fiber suffered significant transmission losses and burn-back after just 1800 pulses

delivered to a single stone sample. Although the severity varied significantly among individual stone samples and stone types, the COM stones, on average, caused more fiber degradation and burnback than the UA stones, presumably because of the higher ablation threshold of the COM stones which translates to higher temperatures needed for ablation. This observation is supported by previous studies using the Ho:YAG laser with larger core standard fibers [22, 44]. Recent Ho:YAG laser studies have also reported that larger fiber core diameters (> 300 μm) experience less fiber tip burn-back than smaller core diameters (< 300 μm) [4], further confirming our results. In summary, tapered fibers provide a more robust fiber tip without compromising stone vaporization efficiency, an important property desired in the ideal laser lithotripsy fiber.

Table 3. Transmission losses and fiber burn-back as a function of fiber tip size and stone type for 1800 laser pulses delivered during TFL lithotripsy.

Fiber	150/300 μm Taper*	150 μm Standard	n
Transmission Loss (%)			
UA	0 %	21.3 ± 26.2 %	10
COM	0 %	64.1 ± 10.8 %	10
Burn-back Loss (mm)			
UA	0 mm	0.3 ± 0.4 mm	10
COM	0 mm	0.6 ± 0.3 mm	10

* No measurable transmission loss or burn-back with the tapered fiber after 20 stones x 1800 pulses / stone = 36,000 pulses.

Irrigation rates through the working port of a flexible ureteroscope with different size and type fibers were also conducted (Table 4). The main objective of this experiment was to demonstrate that the 150/300 μm tapered fiber tip did not significantly impede irrigation rates. The tapered fiber provided an equivalent flow rate to a conventional 150 μm fiber (approximately 85% of flow rate without fiber inserted). The

net effect of the tapered fiber is therefore to provide similar characteristics to a standard 300 µm fiber without compromising the irrigation rates and bending characteristics of a 150 µm fiber. Otherwise, flow rates decrease as the fiber outer diameter increases, as expected and previously reported [45]. Note that the fibers tested in this study had different cladding and jacket specifications based on the manufacturer (Polymicro and Thorlabs), resulting in different outer diameters for a given core diameter, and thus directly translating into different flow rates as well.

Table 4. Irrigation rates through a flexible ureteroscope as a function of fiber diameter

Fiber core/cladding/jacket (µm)	Flow Rate (ml/min)	Flow (%)
No Fiber	46.0 $\pm$ 0.5	100
150 / 163 / 196 (P)	39.2 $\pm$ 0.6	85.1 $\pm$ 1.3
150 / 163 / 300 Taper (P)	38.8 $\pm$ 0.6	84.4 $\pm$ 1.3
100 / 125 / 244 (T)	33.3 $\pm$ 0.3	72.5 $\pm$ 0.6
300 / 327 / 376 (P)	26.4 $\pm$ 0.1	57.4 $\pm$ 0.3
200 / 233 / 411 (T)	24.3 $\pm$ 0.6	52.9 $\pm$ 1.3
270 / 322 / 471 (O)	19.8 $\pm$ 0.3	43.1 $\pm$ 0.6
270 / 326 / 631 (T)	12.0 $\pm$ 0.1	26.1 $\pm$ 0.3
365 / 400 / 738 (T)	6.8 $\pm$ 0.1	14.9 $\pm$ 0.3

P = Polymicro fiber; T = Thorlabs fiber; O = Olympus Holmium Lightguide 270D fiber

Ureteroscope deflection measurements as a function of fiber diameter inserted through the working port of the ureteroscope were also conducted (Table 5). The flexible ureteroscope achieved its maximum primary (268^{o}) and secondary (180^{o}) angles of deflection both with and without the 150/300 µm tapered fiber inserted through the working port. No loss in ureteroscope deflection was observed until fiber core sizes of 200 µm or greater were tested. On a separate note, it should also be mentioned that the rigid 5-mm-length tapered fiber tip is short enough to sit protected inside the rigid, distal

tip of the working port of the endoscope during maneuvering through extreme bending conditions (e.g. lower pole of the kidney), thus potentially preventing fracture of the tip during ureteroscope insertion into the urological tract.

Table 5. Ureteroscope angle of deflection as a function of fiber type and diameter.

Fiber core/cladding/jacket (µm)	Primary Deflection Angle (^{o})	Secondary Deflection Angle (^{o})
No Fiber	268	180
Polymicro Fibers:		
150 / 163 / 190	268	180
150 / 163 / 300 Taper	268	180
300 / 327 / 364	239	157
Thorlabs Fibers:		
100 / 125 / 236	268	180
200 / 233 / 411	260	175
270 / 326 / 624	237	155
365 / 400 / 718	216	122
Olympus Fiber:		
270 / 322 / 464	230	163

4.4 Discussion

This study describes the preliminary *ex vivo* testing of a distal tapered fiber tip during TFL lithotripsy. The 150/300 µm tapered fiber combines the flexibility and irrigation rates of a conventional small-core fiber with the robust mechanical properties of a large-core fiber. The tapered fiber produced comparable stone mass loss to conventional small-core fibers without any evidence of fiber transmission loss or burn-back.

The focus of this study was on the use of small tapered fiber tips (150/300 µm core). However, it should be noted that these fibers can also be fabricated with different

diameters and lengths, depending on the application. For example, 200/400 µm and 200/600 µm tapered fibers with 10-mm-lengths are available and have been tested in our laboratory as well. While the taper length may be variable, there are technical limits for the taper ratio. Typically, a 2:1 taper diameter ratio can be fabricated for smaller fiber diameters and a 3:1 taper ratio for the large fiber diameters, due to the finite volume of silica material that can be drawn and stretched during the tapering process [41].

One major limitation of a distal tapered fiber tip is that it may not be possible to re-cleave and re-use the optical fiber once damage to the tip is experienced. Any cleaving of the fiber tip would by definition shorten the taper length and decrease the taper core diameter, and thus, in effect, negate the advantages of using a tapered fiber tip.

It should also be noted that the exposed silica fiber tips of the tapered fiber are extremely delicate due to their small diameter and tapered shape. The fiber tips will require more mechanical reinforcement with a buffer or jacket material prior to clinical application, to prevent the tips from breaking off during normal mechanical manipulation of the fiber into and out of an ureteroscope. However, this modification can easily be performed on the fibers.

4.5 Conclusions

This preliminary study demonstrates the feasibility of using short distal tapered fiber tips during TFL lithotripsy of human urinary stones, *ex vivo*. Tapered fibers used in this manner may combine some of the advantages of small fibers (flexibility, higher irrigation rates) with the advantages of larger fibers (higher power transmission and increased durability). While more studies are definitely needed, the distal tapered fiber tip may bring the promise of a perfect laser lithotripsy fiber one step closer to reality.

CHAPTER 5: FIBER OPTIC MANIPULATION OF STONES

5.1 Introduction

Previous studies have reported that a cavitation bubble is formed when a laser irradiates a stone submerged in an aqueous environment. This bubble is partly responsible for retropulsion of kidney stones during lithotripsy [7, 9-11]. We have also noticed during retropulsion studies that the stone does not always move away from the fiber tip when irradiated with the laser. Other investigators have also reported that stones will sometimes bounce back and forth against the fiber before moving away from the distal tip [7, 12]. These previous studies have attributed this effect to irregularities in the stone surface and collapse of the cavitation bubble. However, this "suction effect" has only been reported, but not studied in detail. The consistent reproduction and control of this phenomenon, once understood, could eliminate retropulsion of kidney stones and the need to chase stones in the urinary tract.

Currently, stone stabilization devices utilizing numerous designs, including baskets, grasping tools, and "backstop" approaches are used to reduce stone retropulsion and to increase ablation efficiency during Ho:YAG laser lithotripsy [46]. However, these devices occupy valuable space inside the single working channel of the ureteroscope. The objective of this study is to analyze the suction effect and determine its dependence on Ho:YAG laser pulse energy and TFL pulse rate. This study also explores the mechanism responsible for the suction effect.

The suction effect appeared to be dependent on the size of the stone and the amount of energy being delivered in each pulse. This study used stones of similar size and weight to obtain reproducible results. It was necessary to use the PoP phantom stones for this initial study to minimize contributing variables.

5.2 Methods

5.2.1 Laser Parameters

An experimental Thulium fiber laser (TLR 110-1908, IPG Photonics, inc., Oxford, MA) was operated at a wavelength of 1908 nm and was externally modulated with a function generator (DS345, Stanford Research Systems, Sunnyvale, CA) to produce a pulse duration of 500 μs. The TFL was operated at a constant pulse energy of 35 mJ while varying the pulse rate from 10-350 Hz. A clinical Holmium:YAG laser (TwoPointOne XE, Coherent, Santa Clara, CA) was operated at a wavelength of 2120 nm and pulse duration of 300 μs. The Ho:YAG laser was limited to operation at a relatively low pulse rate of 20 Hz while varying the pulse energy from 35-360 mJ.

5.2.2 Stone Suction Experiments

Spherical, 4-mm-diameter, Plaster-of-Paris (PoP) stone phantoms with an average mass of 40.4 ± 2.0 mg were formed using a mold and sandpaper to smooth rough spots. These stones were used as an idealized model to eliminate potential variability due to stone shape and density. Previous investigators have also used PoP stone phantoms to model urinary stones because of their comparable tensile strength [10-11]. Each stone was dried for at least 24 hours and weighed using an analytical balance (AB54-S, Mettler-Toledo, Switzerland). The stones were monitored throughout the suction

experiments, and any damaged stone was removed and replaced. A minimum of 5 PoP stone phantoms were used for each set of laser parameters in all the studies.

Stones were placed in a saline bath on a level, flat surface with ruler markings. Laser energy was delivered through a 270-μm-core optical fiber (Holmium Lightguide 270D, Olympus Gyrus ACMI, Southborough, MA) to the stone. The experiment was recorded with a camera at a frame rate of 30 Hz (73K3HN-YC, Mintron, Fremont, CA). The fiber was positioned parallel to the surface of the saline bath, with energy being delivered to the side of the stone. The fiber was then pulled away from the stone at the maximum speed allowable to maintain stone movement without detachment. Figure 26 shows the experimental setup used to measure the stone velocity. Velocity was calculated by dividing the distance travelled by the time it took to traverse the distance. Figure 27 shows representative images of the initial and final stone locations after pulling for a time of 16 seconds using the Ho:YAG laser at 70 mJ. The average velocity for each set of laser parameters was plotted using the recorded distance and time traveled by the stone. For the TFL, velocity versus pulse rate was plotted. For the Ho:YAG laser, velocity versus pulse energy was recorded.

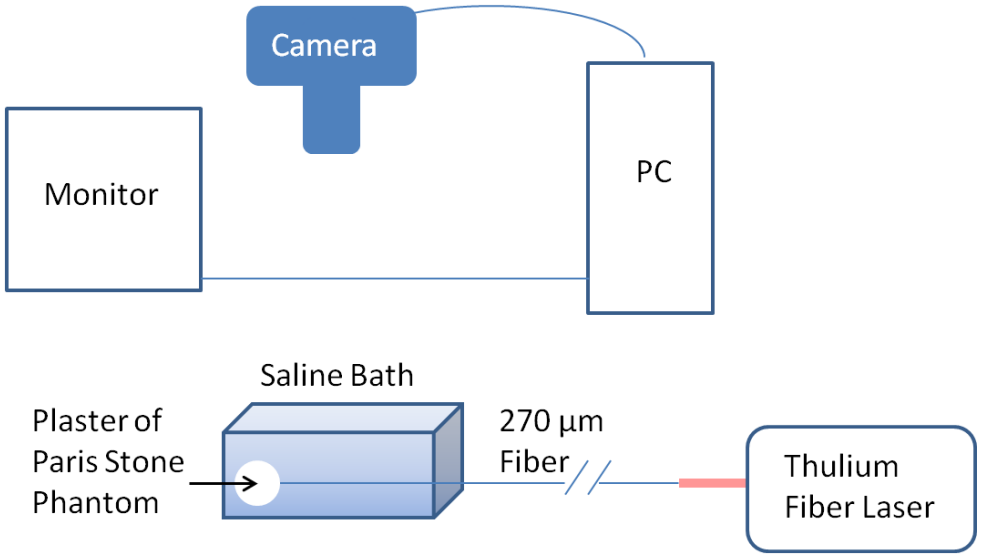

Figure 26. Experimental setup used to record stone movement during laser fiber optic manipulation.

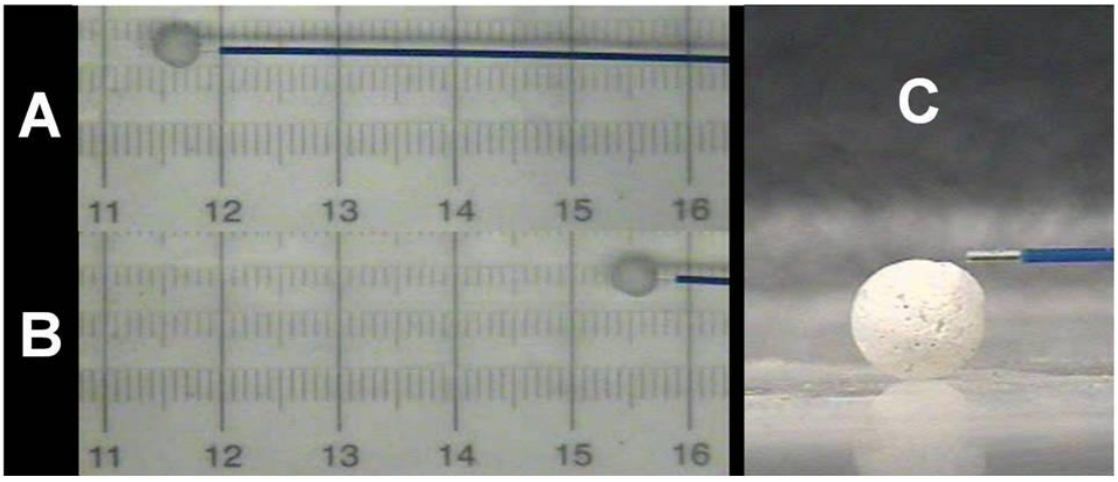

Figure 27. Before (A) and after (B) snapshot of the 4-mm-diameter PoP stone being pulled by the 270-µm-diameter fiber across a ruled surface in a saline bath using the Ho:YAG laser, operating at a pulse rate of 20 Hz and a pulse energy of 70 mJ. (C) Side-view of fiber to stone orientation. Positioning of the fiber tip slightly off-center, above the stone, provided optimal stone manipulation.

5.2.3 Particle Image Velocimetry (PIV)

Polymer microspheres (Duke Standards 4000 Series, Thermo Fisher Scientific, Waltham, MA) with diameters ranging from 30-50 μm, refractive index of 1.59, and density of 1.05 g/cm^3, were suspended in water. The microsphere density closely matched that of the water to ensure suspension in the water bath. The microspheres were illuminated from the side by a fiber optic lamp. A 270-μm-core fiber was inserted in the bath with the length of the fiber level with the surface. Laser energy was delivered in the water bath while videos of particle flow were recorded under magnification. The recorded particle flow was used to map the water flow as a function of the laser parameters. This method examined the macroscopic effects of a train of laser pulses on the water flow.

5.2.4 Thermal Imaging

A thermal camera (SC655, FLIR, Billerica, MA) with a 50 Hz frame rate and 640x480 resolution was used to track the water flow as laser energy was delivered. The water bath was maintained near body temperature (~37°C). Similar to the PIV experiments described above, a 270-μm-core fiber was inserted in the water bath with the length of the fiber level with the surface. Videos of the thermal signatures were recorded for TFL pulse rates of 10, 50, 100, 200, and 350 Hz. The thermal signature videos were compared to those using the microspheres as an alternative method to visualize the water flow caused by laser energy delivered in the water bath.

5.3 Results

5.3.1 Stone Suction Experiments

For the TFL, the effect of a net force pulling the stone towards the trunk end of the fiber was noticeable even at a low pulse energy and pulse rate of 35 mJ and 10 Hz (Figure 28a). The effect was weak, and no stone retropulsion was observed. As the pulse rate was increased, the effect of the force pulling the stone towards the fiber tip became stronger. The pull velocity of the stones increased up to 250 Hz (although the increase between 75-250 Hz was not statistically significant). Each pulse caused the water to flow in two different directions. The water flow increased as the pulses were delivered more rapidly at higher pulse rates. The compounding effects of forces from each pulse acted on the stone by either pushing or pulling it away from the fiber tip, depending upon where the fiber tip was placed with respect to the stone.

As the pulse rate was increased up to 250 Hz, strong retropulsion forces were observed. This was a problem when trying to keep the stone attracted to the fiber tip. Because the effect of pulling or pushing the stone is dependent upon where the fiber tip is placed, when the net retropulsive force begins to dominate, the location of the fiber tip is critical. This may be the cause for the high error bars in the mid-range pulse rate data points shown in Figure 28. Both retropulsion and attraction forces were acting on the stone, and it was difficult to control which force dominated in the 200 Hz range.

As the pulse rate was further increased to 350 Hz, retropulsion forces dominated. The stone was not pulled as far without eventually being rapidly pushed away. One of the reasons for this effect is that the retropulsion forces were so strong that a tightly wound vortex (to be seen in the PIV experiments) developed in close proximity to the

fiber tip. The attractive forces were overcome by this vortex and the stone was caught in the jet pushing away from the fiber tip.

The trend was similar for the Ho:YAG laser (Figure 29). As the pulse energy was increased, the stone velocity also increased until ~210 mJ (although the increase was not statistically significant for pulse energies between 70-210 mJ). The stone velocity then decreased as the pulse energy increased beyond 210 mJ. For operation at 35 mJ, the suction effect was observed without any retropulsion effects. As the pulse energy was increased, the stone was pulled more rapidly, but in a discrete, choppy pattern of motion. The process of pulling the stone was not smooth as experienced with the TFL. Use of higher pulse energies above 70 mJ resulted in greater retropulsion, which required the fiber to be held further away from the stone to maintain the suction effect. At pulse energies above 210 mJ, the stone bounced randomly in all directions and retropulsion was increasingly difficult to avoid. Pulse energies at 300 mJ and higher yielded a much different result than lower energies. The stone was either pushed far ahead of the fiber tip or pushed far behind the fiber tip in a quick, discrete motion. The attractive force at higher pulse energies required the fiber to be placed completely past the stone, with the potential risk of the laser energy delivered by the fiber being absorbed by tissue structures directly in front of the fiber.

Figure 30 shows the stone average velocity as a function of average power. This plot provides a direct comparison between the Ho:YAG and TFL. The TFL was able to exploit the suction effect at more than double the power produced by the Ho:YAG laser. More power delivery makes it possible for the TFL to potentially exploit the suction

effect to maximize stone ablation rates while at the same time minimizing stone retropulsion.

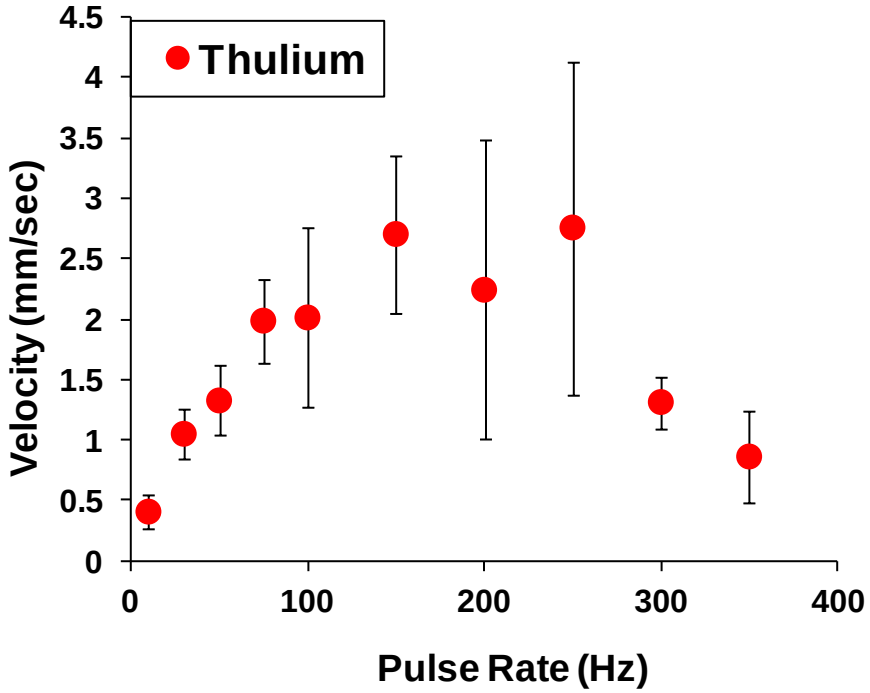

Figure 28. Velocity of stones pulled using the TFL as a function of pulse rate for pulse energy of 35 mJ.

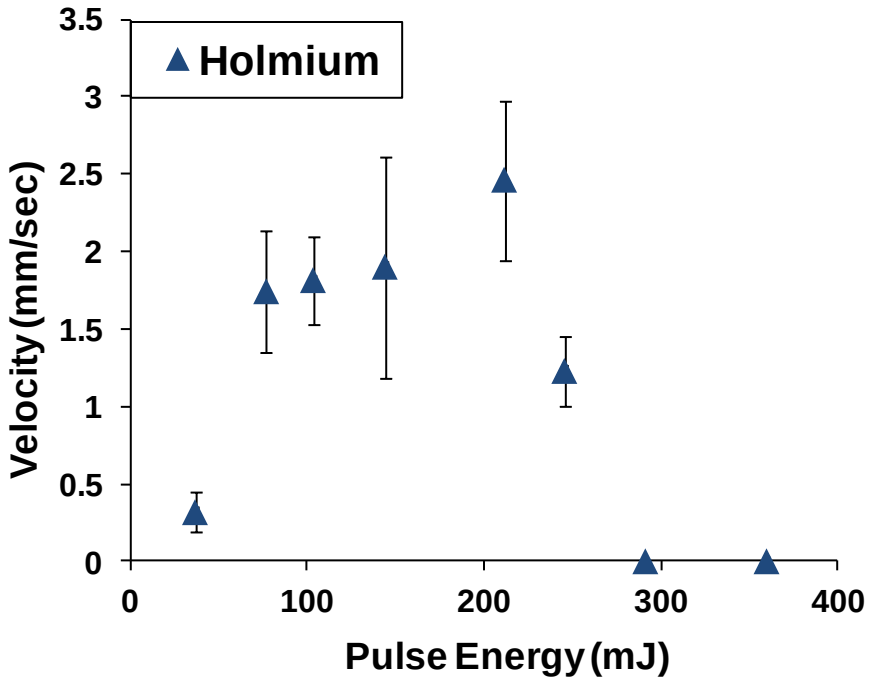

Figure 29. Velocity of stones pulled using the Ho:YAG as a function of pulse energy for pulse rate of 20 Hz.

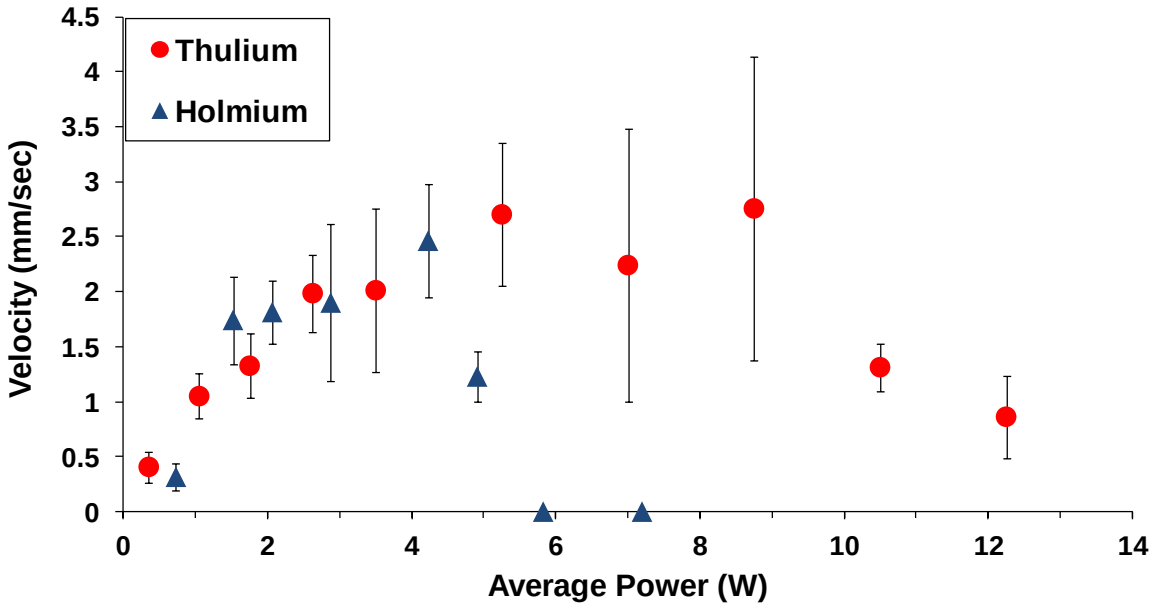

Figure 30. Stone velocity pulled for both lasers as a function of average power.

5.3.2 Particle Image Velocimetry

Microspheres ranging from 30-50 μm in diameter were used to track the water flow during laser irradiation with both the TFL and Ho:YAG lasers. The results of our study show two dominating but opposing forces during lithotripsy. One force, a retropulsive force, is away from the fiber tip. The other force, an attractive force, is towards the fiber tip. The attractive force is suspected to be the cause of the suction effect observed during laser irradiation with both the TFL and Ho:YAG lasers.

Figure 31 illustrates the change in flow of the microspheres as the TFL pulse rate was increased. As the TFL pulse rate was increased, the water flow pattern began to change. At low pulse rates, the microspheres flowed in two directions, towards and away from the fiber tip (Figure 31A). As pulse rates were increased, a vortex began to form around the sides of the fiber, causing microspheres pulled towards the fiber to return and become trapped in the jet flowing away from the fiber (Figure 31B). At pulse rates above 250 Hz, the vortex surrounding the end of the fiber tip became tightly wound around the fiber tip (Figure 31C). This caused microspheres flowing towards the fiber tip to get trapped and then pushed back into the flow away from the fiber tip. This chaotic, tightly wound vortex, is suspected to be the primary cause of decreasing stone velocity at higher pulse rates in the suction effect experiments.

The effects of the forces from the Ho:YAG laser were more clear and consistent with those of the TFL operating at 20 Hz with regard to the flow of microspheres. The vortices seen at higher pulse rates using the TFL were not seen using the Ho:YAG as pulse energies were increased. This could be due to the attractive force becoming stronger at roughly the same rate as the retropulsive force. The experiments using the

Ho:YAG showed that the speed in which the spheres moved away from the fiber tip, in both directions, increased as the pulse energy was increased.

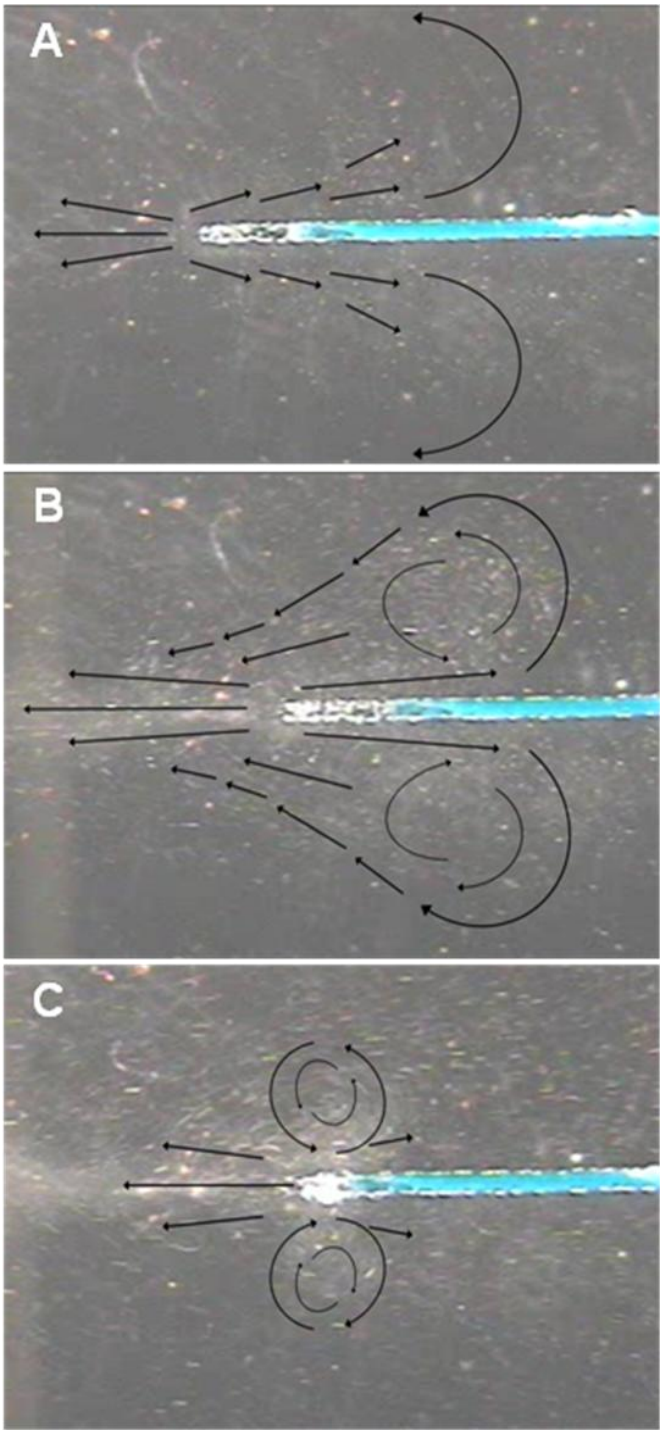

Figure 31. The flow of microspheres for TFL pulse rates of A) 20 Hz, B) 200 Hz, and C) 350 Hz at 35 mJ per pulse.

Although the frame rate of the camera used to capture the flow of microspheres was limited to 30 Hz, it was able to capture the shockwave-induced photoluminescence resulting from the collapse of the cavitation bubbles created by both TFL and Ho:YAG (Figure 32). Such a distinct signature of cavitation bubbles has been previously reported as well [47-48]. Figure 32 also shows distinct differences in the shape and formation of cavitation bubbles created using the TFL (A) and the Ho:YAG (B).

The modulated TFL operates at a longer pulse length (500 μs) than the Ho:YAG (300 μs). Furthermore, the absorption coefficient of water at the TFL wavelength (μa= 160 cm-1) is five times greater than that of the Ho:YAG (μ_a= 28 cm^{-1}) [42]. Previous investigators have shown that for both increased absorption and longer pulse durations, the cavitation bubble becomes elongated and multiple cavitation bubbles may form [24, 29, 49]. Evidence of this is seen in the results for the TFL microsphere experiments. Photoluminescence of shockwaves was observed emanating from two distinct points in front of the fiber tip (Figure 32A).

The Ho:YAG induced cavitation bubbles have been shown to be less elongated and pear shaped. This is evident from the results of the microsphere study performed with the Ho:YAG laser (Figure 32B). The area of photoluminescence appeared oval and resembled the shape of Ho:YAG induced cavitation bubbles reported by other investigators [11, 24, 29, 50-51].

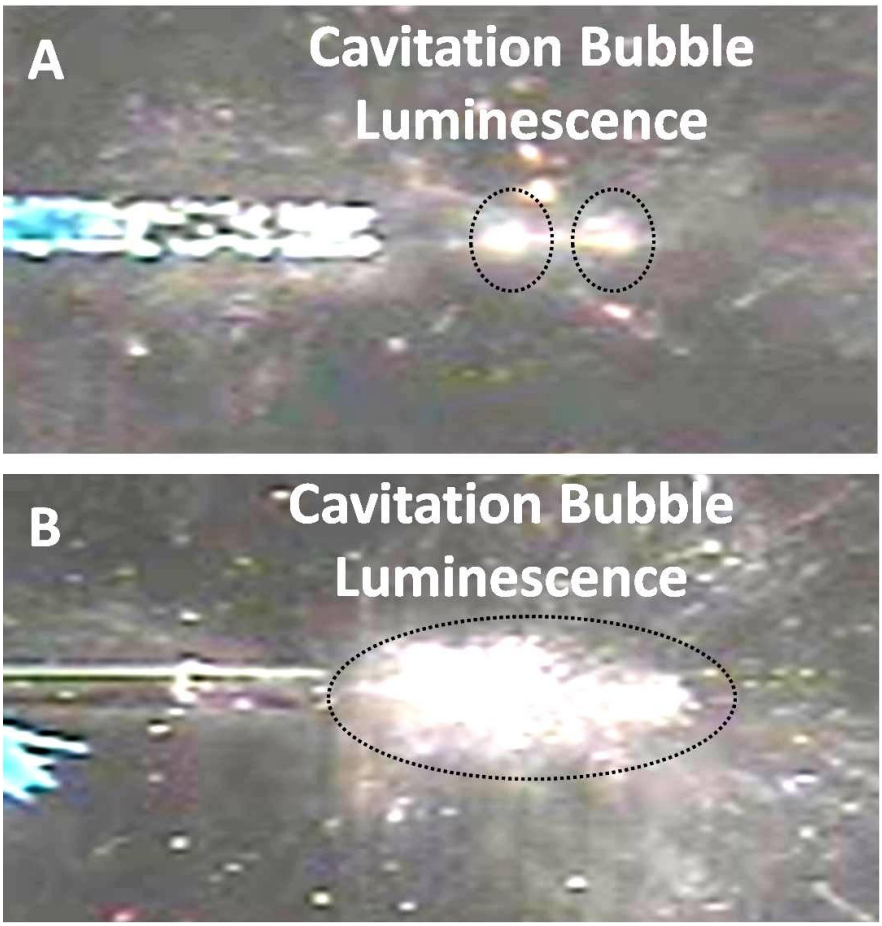

Figure 32. Photoluminescence of shockwave resulting from the collapse of cavitation bubbles for A) TFL pulse rate of 350 Hz at 35 mJ pulse energy and B) Ho:YAG pulse rate of 20 Hz at 300 mJ pulse energy.

5.3.3 Thermal Imaging

A thermal camera was used to track the water flow as laser energy was delivered just beneath the surface of the water bath. For the TFL, the camera recorded a flow of thermal energy away from the fiber tip and towards the trunk end of the fiber. The thermal camera also recorded small thermal eddies near the fiber tip. Figure 33 shows a frame of an image captured. The only noticeable trend in thermal images as the TFL pulse rate increased was that the area of thermal flow also increased. Thermal images

(not shown here) were also captured using the Ho:YAG laser, but no discernible trend was observed, possibly due to the longer optical penetration depth of the Ho:YAG wavelength in water. The videos captured with the thermal camera reinforced the validity of trends observed in the suction effect and particle velocimetry studies.

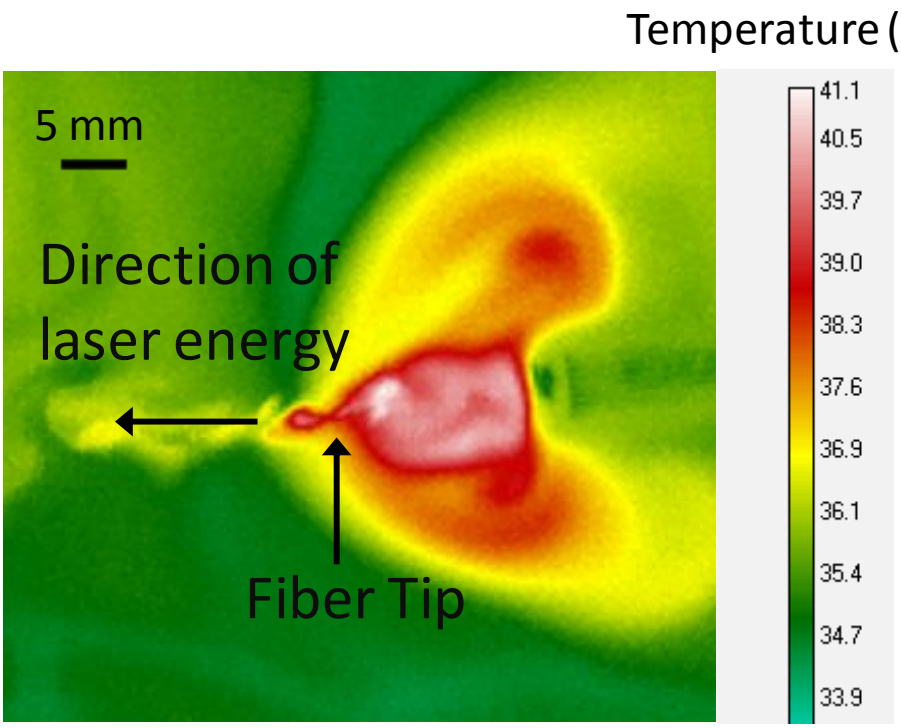

Figure 33. Frame of a thermal video captured during fiber optic delivery of the TFL energy at 35 mJ and 200 Hz in a water bath (color image).

5.4 Discussion

Previous investigators have reported the role of cavitation bubble dynamics during Ho:YAG laser lithotripsy [8, 11, 22, 29, 32]. Images show small residual effects of the bubble collapse behind the tip of the fiber [11, 51]. This is presumably due to a collapsing bubble induced pressure wave propagating in the axial direction of the fiber,

both towards and away from the fiber tip. While this pressure wave has been observed to be too weak to induce photomechanical ablation of urinary stones, it has been shown to be sufficiently strong to push stones away from the fiber tip. This study investigated in further detail the pressure wave reported in previous studies that may be responsible for the suction effect [32, 51-54]. A recent study has also reported that during the collapse of micrometer-sized bubbles the maximum pressure of the shock wave emitted during bubble rebound can be an order of magnitude smaller than that induced by millimeter-sized bubbles [55]. Future studies utilizing a high speed camera for direct imaging of cavitation bubble dimensions and dynamics during both Ho:YAG and TFL lithotripsy may address how large the bubble must be in order to observe the suction effect.

There are many potential uses for the suction effect. The most direct use would be to manipulate urinary stones in the kidney or bladder. Because the TFL is able to produce the suction effect at pulse rates that do not result in retropulsion, a stone could be trapped at the fiber tip and then transported to a more desirable location for stone ablation. If the stone is sufficiently small, the suction effect could also be used to navigate the stone out of the urinary tract. Furthermore, when using the TFL, the suction effect is dominant over retropulsion at pulse rates ideal for stone ablation (up to 150 Hz). This may provide the possibility of trapping the stone at the fiber tip during stone ablation. Ideally, the stone would bounce around the tip of the fiber while it is broken down. Overall, exploitation of the suction effect would provide an urologist with greater control during laser lithotripsy without the need for stone stabilization devices.

While the reproduction and quantification of the suction effect is possible, it requires further study. Our results show high error bars, mainly due to human error in

positioning the fiber in the most efficient location relative to the stone to utilize the suction effect. An urologist may have even less control positioning the fiber around the stone. This limitation must be overcome before the suction effect can be viable for surgical application. Also, based on experimental observations, the suction effect is dependent upon the size of the stone. The effect is not as strong as the size of the stone increases. The shape of the stone may also play a role in the strength of the suction effect. Finally, our studies were performed in a stable environment. The drag force of motionless saline was the only major force acting against the stone. Other forces, such as the flow of saline through the working channel of the ureteroscope, may play a significant role in whether or not the stone can be trapped by the attractive forces responsible for this suction effect.

5.4 Conclusions

This study has demonstrated the ability of both the Holmium:YAG and Thulium fiber lasers to rapidly and reproducibly pull stone phantoms. Our knowledge of the suction effect is not yet sufficient for use in practical applications. Further studies need to be conducted to overcome these current limitations. Pulse duration, pulse energy, pulse distribution, stone size, stone shape, and environment all need to be further explored. Future studies should also include calculations of forces acting on the stones and the effect of water turbulence during the procedure. Future work may focus on the role of this “suction effect” as a tool to manipulate urinary stones during laser lithotripsy. This phenomenon may also ideally be used to trap stone fragments during ablation, thus potentially eliminating the need for a stone stabilization device.

CHAPTER 6: TFL LITHOTRIPSY USING PULSE TRAIN MODULATION

6.1 Introduction

Laser lithotripsy using low pulse energies (< 0.5 J) and high pulse repetition rates (> 20 Hz) has been demonstrated to be preferable to the use of high pulse energies (1-2 J) at low pulse rates (< 10 Hz) [22-23], when stone retropulsion is a primary concern. However, this approach, while reducing stone retropulsion, may also come at the expense of slower stone ablation rates, which may be only partially compensated for by the use of higher pulse rates, thus potentially increasing operation time in the clinic.

The diode-pumped TFL has the interesting potential to more easily control and vary the pulse characteristics into packaged bursts of micro-pulse trains (MPT), than does the conventional flashlamp-pumped Ho:YAG laser technology. Therefore, the potential of this variation in traditional pulse delivery to impact laser lithotripsy is explored in this study. More specifically, the objective of this study is to determine whether TFL delivery of micro-pulse trains may result in improved stone ablation rates, which would in turn translate into reduced operation times in the clinic. Application of bursts of short laser pulse trains has previously been shown to increase material removal for both laser processing of metals [56] and soft tissues [57-58]. However, in the field of urology, investigators have only recently studied a similar approach for Ho:YAG laser lithotripsy using longer pulse lengths, and without significant results [59]. In this study, application of Thulium fiber laser micro-pulse trains are explored for enhanced laser lithotripsy.

6.2 Methods

6.2.1 Stone Sample Preparation

Human uric acid (UA) and calcium oxalate monohydrate (COM) urinary stone samples with purity greater than 95% were obtained from two stone analysis laboratories (Louis C. Herring & Co, Orlando, FL and Labcorp, Oklahoma City, OK) and the Carolinas Medical Center (clinic of P. Irby) and used for the ablation rate and fiber burn-back studies. The stones were immersed in a saline bath and kept fixed in place during the lithotripsy experiments.

6.2.2 Laser Parameters

An experimental Thulium fiber laser (TLR 110-1908, IPG Photonics, inc., Oxford, MA) was externally modulated with a function generator (Model DS345, Stanford Research Systems, Sunnyvale, CA) to operate in pulsed mode with a wavelength of 1908 nm, pulse energy of 35 mJ, 500-μs pulse duration, and pulse rates of 10-50 Hz. A pulse energy of 35 mJ was used for all of the studies because it was the maximum output pulse energy achievable from the TFL and optical fiber used in these studies for a 500 μs pulse duration. The laser energy was delivered through a standard 100-μm-core, low-OH silica optical fiber (AFS105/125Y, Thorlabs, Newton, NJ) for all of these studies. This fiber has a smaller core diameter and was not sterilized, but otherwise it is of similar composition to the fibers used in the clinic with the Ho:YAG laser.

The TFL was operated at 1908 nm, 35-mJ pulse energies, and 500-μs pulse duration, in a train of 5 micro-pulses, and macro-pulse rates of 10 Hz (Figure 34). The ablation results from this micro-pulse train were directly compared with conventional

macro-pulse TFL operation at 10, 30, and 50 Hz. The urinary stone samples were dried by heating them to 60^{o}C for 30 min, and then cooled to room temperature in a container filled with desiccant before and after each experiment. Stone mass loss was measured using an analytical balance (AB54-S, Mettler-Toledo, Switzerland), and mass loss rates were calculated by dividing this value by the total number of pulses and total irradiation time.

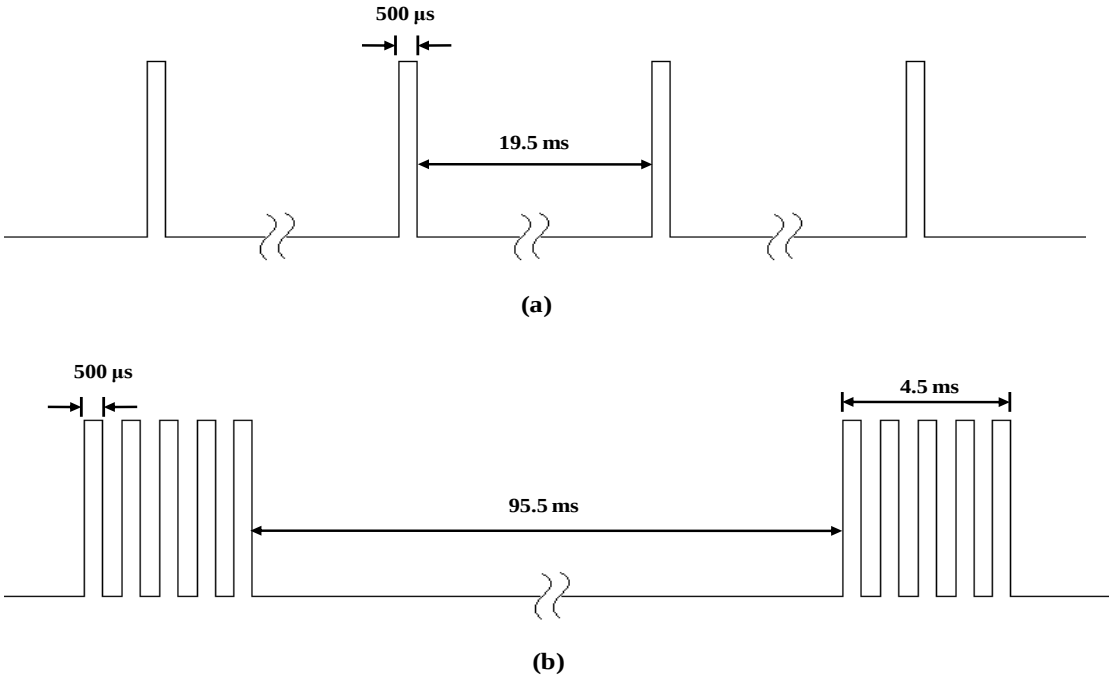

Figure 34. Diagram comparing Thulium fiber laser pulse delivery modes. (a) Standard pulse mode consisting of 500 µs pulse length and a pulse repetition rate of 50 Hz; (b) Micro-pulse train mode consisting of a packet of five standard 500 µs long pulses, with an overall pulse rate of 10 Hz. Each configuration (a,b) delivers the same total number of pulses (50) per second and the same total energy to the urinary stone. Each individual pulse delivers 35 mJ to the stone.

6.2.3 Optical Imaging of Ablation Craters

Imaging of the urinary stone ablation craters after Thulium fiber laser lithotripsy was performed using a light microscope (FS70, Mitutoyo America, Aurora, IL) to observe the ablation crater dimensions at the stone surface. Optical Coherence Tomography (OCT) of the stone samples was also performed to image the cross-sectional profile of the ablation crater. An endoscopic OCT system (Niris, Imalux, Cleveland, OH) with 7-Fr probe was used for the studies, providing images of 2.0 mm width by 1.6 mm depth, with an axial resolution of 11 μm and a lateral resolution of 25 μm in tissue.

6.2.4 Fiber Tip Degradation Studies

For each group of laser parameters, each stone sample received a total of 6000 pulses corresponding to a total energy of 210 J. Fiber tip burn-back during lithotripsy was quantified, simply by placing markers on the fiber and then measuring under magnification the loss in length at the distal fiber tip, to the nearest 100 μm, after the lithotripsy procedure was completed.

6.2.5 Stone Phantom Retropulsion Studies

Laser energy was delivered through 100-μm-core optical fibers in contact mode with 6-mm-diameter Plaster-of-Paris (PoP) stone phantoms, submerged in a saline bath. Spherical PoP stone phantoms having approximately the same size (6-mm-diameter) and density as urinary stones were created using a mold, and then used for the stone retropulsion studies as a model for providing more reproducible results than the irregularly shaped human stone samples. A rigid ureteroscope (9.5-Fr ID, Karl Storz, Germany) attached to a light source (X7000, Stryker Endoscopy, San Jose, CA), camera (1188HD, Stryker), and monitor, was used to accurately position the optical fiber tip so

that it was perpendicular to, centered on, and in contact with the PoP stone phantom prior to irradiation (Figure 35). Stone retropulsion distance was measured for each set of laser parameters, for a fixed total number of pulses (1200) and total energy (42 J) delivered to the stone.

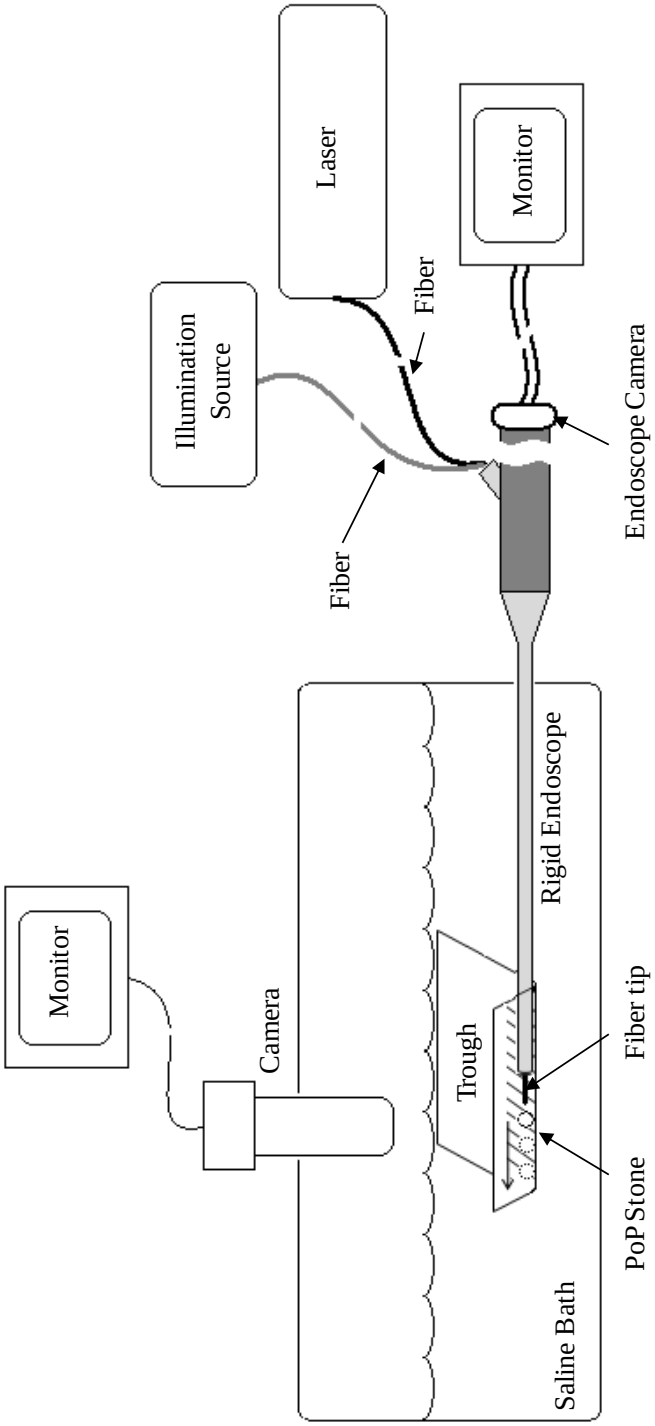

Figure 35. Diagram of experimental setup for measuring stone retropulsion distances during Thulium fiber laser lithotripsy. Plaster-of-Paris (PoP) stone phantoms were used as a stone model to provide a reproducible sample in terms of mass, shape, and stone retropulsion).

6.2.6 Data Analysis

Stone ablation mass loss, fiber burn-back, and stone retropulsion were reported as a mean $\pm$ the standard deviation (S.D.). A minimum of five samples were tested for each data set. A Student's T-test was performed to determine statistical significance between micro-pulse train and standard (50 Hz) pulse train data sets for each study (ablation mass loss, fiber burn-back, and stone retropulsion). A value of $P < 0.05$ was determined to be statistically significant.

6.3 Results

6.3.1 Stone Ablation Rates

The stone ablation rates (μg/s) for Thulium fiber laser lithotripsy are provided in Table 6, as a function of stone type and pulse delivery mode. As anticipated, stone mass removal increases as the pulse rate is increased from 10-50 Hz for the standard pulse mode. However, TFL operation in MPT mode resulted in a factor of two increase in the stone mass removal rate of 414 $\pm$ 94 μg/s and 122 $\pm$ 24 μg/s for the UA and COM stones, respectively, compared to 182 $\pm$ 69 μg/s and 60 $\pm$ 14 μg/s with individual pulses delivered at 50 Hz, for the same number of pulses delivered (UA: $P = 0.00006$; COM: $P = 0.00009$). Optical coherence tomography cross-sectional images and light microscopy of the surface show larger stone ablation crater dimensions for MPT mode versus the standard pulse train, for both the UA and COM stone samples (Figure 36 and Figure 37). The crater depths and widths using the micro-pulse packets are roughly double in size of those using the standard pulse train, thus reinforcing the results of the ablation rate study.

Table 6. Mean ablation rates (μg/s) for Thulium fiber laser lithotripsy as a function of stone type and pulse delivery mode.

Pulse Train	UA	COM
Standard Pulse:		
10 Hz	51 ± 13	18 ± 2
30 Hz	117 ± 31	41 ± 12
50 Hz	182 ± 69	60 ± 14
Micro-Pulse Train:		
5 pulse packet at 10 Hz	414 ± 94	122 ± 24

* The pulse energy was 35 mJ, pulse duration was 500 μs, fiber diameter was 100 μm, and total number of pulses was 6000. N ≥ 5 samples for each data set.

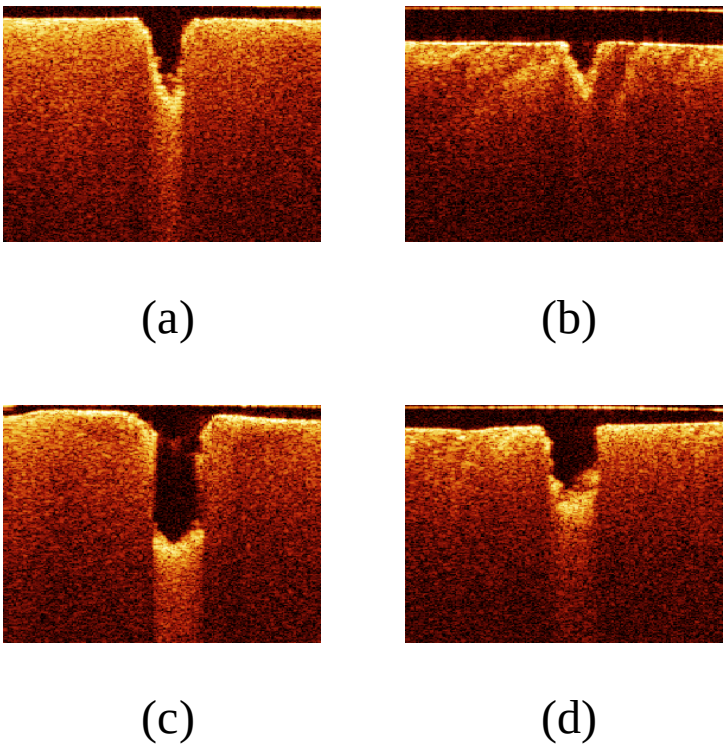

Figure 36. Representative optical coherence tomography images of uric acid (UA) and calcium oxalate monohydrate (COM) stone samples after Thulium fiber laser lithotripsy. The first row of images shows cross-sectional (width x depth) ablation craters using standa rd pulse mode (500 μs pulses at 50 Hz) for a total of 50 pulses delivered to the stone sample: (a) UA stone; (b) COM stone. The second row of images shows ablation craters for a micro-pulse train consisting of a packet of five 500 μs pulses, with an overall pulse rate of 10 Hz, also for a total of 50 laser pulses delivered to the stone sample: (c) UA stone; (d) COM stone. The micro-pulse train (bottom row) produces larger ablation craters than the standard pulse (top row) for both UA and COM stone types. Scale of images (2 mm width x 1.6 mm depth).

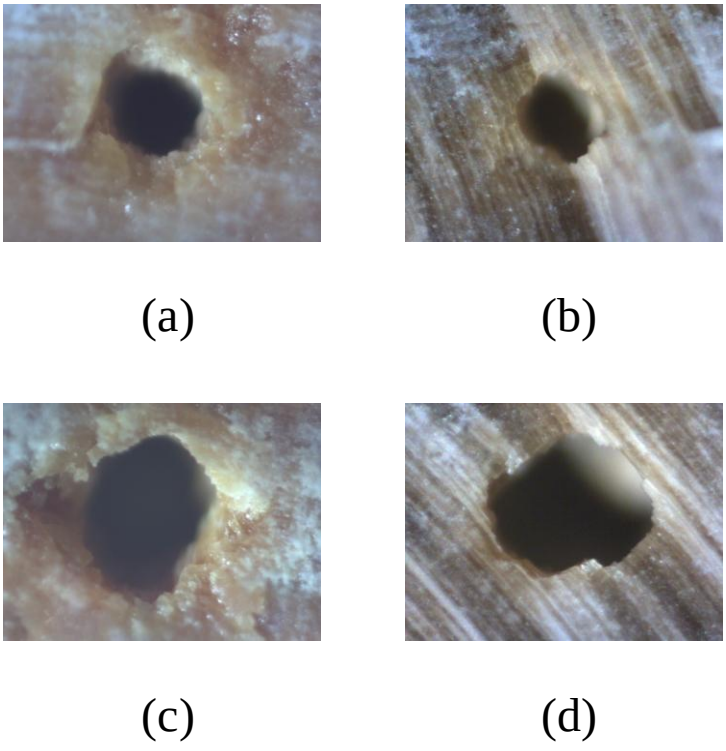

Figure 37. Representative light microscopy images of uric acid (UA) and calcium oxalate monohydrate (COM) stone samples after Thulium fiber laser lithotripsy. The first row of images shows ablation craters using standard pulse mode (500 μs pulses at 50 Hz) for a total of 50 pulses delivered to the stone sample: (a) UA stone; (b) COM stone. The second row of images shows ablation craters for a micro-pulse train consisting of a packet of five 500 μs pulses, with an overall pulse rate of 10 Hz, also for a total of 50 laser pulses delivered to the stone sample: (c) UA stone; (d) COM stone. The micro-pulse train (bottom row) produces larger ablation craters than the standard pulse (top row) for both UA and COM stone types. Scale of images (700 μm width x 500 μm height).

6.3.2 Fiber Tip Degradation Studies

Degradation to the fiber tip was also quantified during the ablation studies as a function of stone type and pulse delivery mode, simply by measuring the amount of fiber burn-back that occurred during lithotripsy (Table 2). Fiber burn-back was significantly higher for COM stones than UA stones, and also increased with pulse rate. The MPT

mode produced less burnback than the 50 Hz standard pulse train (UA: P = 0.01; COM: P = 0.04).

Table 7. Fiber burnback (mm) for Thulium fiber laser lithotripsy as a function of stone type and pulse delivery mode.

Pulse Train	UA	COM
Standard Pulse:		
10 Hz	0.9 ± 0.8	1.3 ± 0.4
30 Hz	1.1 ± 0.7	2.0 ± 0.4
50 Hz	1.0 ± 0.7	3.4 ± 0.5
Micro-Pulse Train:		
5 pulse packet at 10 Hz	0.3 ± 0.4	2.9 ± 0.4

* The pulse energy was 35 mJ, pulse duration was 500 μs, fiber diameter was 100 μm, and total number of pulses was 6000. N ≥ 5 samples for each data set.

6.3.3 Stone Phantom Retropulsion Studies

Plaster-of-Paris stone phantoms were used to study stone retropulsion as a function of stone type and pulse delivery mode (Table 3). The retropulsion distance measured after delivery of 1200 pulses was greater for the micro-pulse train (1.3 ± 0.8 mm) than for the standard pulse train (0.6 ± 0.4 mm) (P = 0.007). However, retropulsion for both pulse modes was considered to be minimal, based on criteria which will be discussed further below.

Table 8. Retropulsion distance (mm) of Plaster of Paris stone phantoms for Thulium fiber laser lithotripsy as a function of pulse profile.

Pulse Profile	Retropulsion (mm)
Standard Pulse:	
50 Hz	0.6 ± 0.4
Micro-Pulse Train:	
5 pulse packet at 10 Hz	1.3 ± 0.8

* The pulse energy was 35 mJ, pulse duration was 500 μs, fiber diameter was 100 μm, and total number of pulses was 1200. N = 10 samples for each data set.

6.4 Discussion

6.4.1 Stone Ablation Rates

For the laser pulse lengths used in this study, on the microsecond timescale, laser lithotripsy is primarily based on a photothermal mechanism [32]. Water is the dominant absorber at the infrared TFL wavelength used in this study, and the bound water in the urinary stone and the surrounding fluid environment in the urinary tract contribute significantly to laser ablation efficiency. In general, stone ablation is achieved by rapid superheating of the water and surrounding stone material to ablative temperatures through the absorbed laser energy. There is no reason to believe that a standard pulse mode inherently results in optimal transfer of the laser energy into the ablative process. Alternative pulse mode schemes may produce higher ablation efficiencies, resulting in more rapid stone removal.

In this study, TFL lithotripsy in MPT mode resulted in a factor of two increase in ablation rates compared to standard pulse mode for both UA and COM stones, for the same pulse rate (50 Hz) and total number of pulses (6000) delivered to the stones. One possible explanation for this result is that the standard pulse train at 50 Hz produces very little thermal buildup in the stone sample in between pulses, while the MPT mode produces a rapid, stacked pulse sequence resulting in thermal buildup within the stone sample and enhanced stone ablation, but also sufficient cooling between micro-pulse trains to avoid excessive stone charring. Any attempt to increase TFL ablation mass loss by simply increasing the TFL pulse energy and pulse length using the standard pulse mode is not feasible because it produces excessive charring of the stone, accelerated fiber burn-back, and increased stone retropulsion, as observed during previous studies.

It is possible that further exploration of the interaction between laser pulse length, duty cycle, and pulse repetition rate parameters for both the individual micro-pulses and the macro-pulse envelope of the MPT mode could result in an even greater improvement in the ablation rate. However, for this preliminary study, we were limited to operation at a 1:1 duty cycle (On: 500 μs / Off: 500 μs) for the micro-pulse sequence, and also to individual micro-pulse energies of equal magnitudes (35 mJ). With improved flexibility in pulse generation and modulation of the laser, variation of these parameters may also play an important role in optimization of TFL stone ablation rates.

Furthermore, it should be noted that TFL technology is currently limited to operation in short-pulse mode (e.g. nanosecond pulse lengths) or CW mode with the option of external modulation, as used in this study. Thus, pulse lengths are either too short or too long for direct comparison with the Ho:YAG laser lithotriptor, which has pulse lengths on the order of 350-700 μs. Therefore, the objective of this preliminary study was to determine whether stone ablation mass loss could be increased by using custom micro-pulse trains within the limitations of external modulation for pulsed mode of operation from a CW TFL laser.

The TFL was limited to operation with a maximum pulse energy of 35 mJ for the 500 μs pulse duration used in these studies. The TFL pulse energy may appear significantly lower than typical minimum Ho:YAG laser pulse energy settings of ~ 400 mJ provided by clinical laser systems used with 200-μm-core fibers. However, the 100-μm-core fibers used in these TFL lithotripsy studies compensated for the low pulse energy by providing an energy density more comparable with Ho:YAG laser lithotripsy. For example, the radiant exposure for TFL lithotripsy was ~ 446 J/cm^2, compared with

the Ho:YAG radiant exposure of ~ 1273 J/cm^2 in the clinic. When the (factor of four) lower stone ablation threshold for the TFL compared to the Ho:YAG laser is also factored in, the 35 mJ pulse energy delivered through a 100-μm-core fiber translates into a comparable range of parameters for TFL lithotripsy to that of the Ho:YAG laser. The radiant exposures used in this study are also well above the TFL ablation thresholds previously measured for UA (6.5 J/cm^2) and COM stones (20.8 J/cm^2), which is required for efficient and rapid lithotripsy.

Finally, previous reports have shown that the beam profile emitted from a small diameter fiber (e.g. 100-μm-core) may produce a different irradiance along its optical axis than the beam profile from a larger multimode fiber (e.g. 200-μm-core) because of the presence of higher order mixed modes [60]. Normally, the spatial beam profile would need to be considered in any comparisons using different fiber diameters. However, during laser lithotripsy the fiber tip is in constant contact with the stone, and the fiber tip experiences rapid degradation from ablative stone fragments. As a result, the spatial beam profile out of the fiber is constantly changing and difficult to quantify. Nevertheless, in summary, the radiant exposures used in this preliminary TFL lithotripsy study are well above previously reported UA and COM stone ablation thresholds.

6.4.2 Fiber Tip Degradation Studies

The relatively large amount of fiber burn-back experienced in all of these studies is most likely due to the delicate nature of the 100-μm-core fiber tip, despite the pulse energy being kept low. Smaller optical fiber tips have previously been shown to experience greater burn-back for both the TFL and Ho:YAG lasers during lithotripsy [39]. For a given set of laser parameters, fiber burn-back was also consistently less for

UA stones than for COM stones, presumably due to the softer composition and smoother surface of the UA stones. On the contrary, the COM stones exhibited a more irregular surface which increased the probability of the fiber tip becoming lodged and damaged in the stone crevices.

The phenomenon of fiber burn-back should be put into proper perspective. It was previously stated that the initial spatial beam profile at the distal end of the fiber tip during Ho:YAG laser lithotripsy is usually destroyed due to impact of ablative stone fragments early in the lithotripsy procedure since the fiber is in contact mode with the stone. Additionally, the sterile clinical fibers are typically designated as disposable, single-use fibers. However, a high amount of fiber burn-back during an individual lithotripsy procedure may be clinically significant. For example, if bleeding (although rare) occurs during laser lithotripsy, continuous irrigation is necessary to keep the visual field clear. However, if the surgeon has to pause frequently to recleave a damaged fiber tip, blood clots can form quickly and vision may become obscured, in turn leading to increased operative times and potentially lower stone free rates.

6.4.3 Stone Phantom Retropulsion Studies

Stone retropulsion is a major side-effect of laser lithotripsy because it results in the urologist wasting significant operative time chasing the stone within the urinary tract, effectively reducing the stone ablation efficiency in the process. Less retropulsion would therefore be a desirable feature of a laser lithotripter. In this study, stone retropulsion remained minimal (less than 2 mm after 1200 pulses) for both pulse modes. The amount of stone retropulsion that would be considered acceptable in a clinical study is not easy to quantify. However, for the purposes of this study and previous studies, minimal

retropulsion was defined to be a retropulsion distance of less than 2 mm. This value is based in part on the observation that the fiber tip to stone surface working distance needs to be relatively short, requiring near-contact working conditions, for efficient stone vaporization during laser lithotripsy. Otherwise, large gaps in the fiber-to-stone working distance results in significant absorption of the laser radiation by the intervening water layer and a corresponding decrease in ablation efficiency.

The weak retropulsion effects observed in this study may be explained by both the low pulse energy (35 mJ) and the small optical fiber diameter (100 μm) used in these experiments. Previous Ho:YAG laser lithotripsy retropulsion studies have also reported that the use of lower pulse energies, longer pulse durations, higher pulse rates, and smaller optical fiber diameters is the optimal combination of laser parameters for minimizing stone retropulsion [7-12]. The TFL technology is ideally suited for operation with this combination of laser parameters.

6.5 Conclusions

Thulium fiber laser operation in micro-pulse train mode results in a factor of two increase in the ablation rate compared with standard pulse mode for uric acid and calcium oxalate monohydrate urinary stones, with minimal stone retropulsion. With further optimization, Thulium fiber laser ablation rates may approach values comparable to Holmium:YAG ablation rates in the clinic.

CHAPTER 7: TFL LITHOTRIPSY USING A DETACHABLE FIBER TIP

7.1 Introduction

The superior beam quality of the TFL allows for coupling of the laser radiation into smaller fiber core diameters than with the Ho:YAG laser. The ability to couple high power mid-infrared laser radiation into these smaller fibers introduces several advantages compared to the conventional Ho:YAG laser. As shown in Table 5 in Chapter 5, optical fibers with core diameters greater than or equal to 200 µm hinder the deflection of the flexible endoscope when inserted into the working channel of the endoscope. Thus, for optimal use of the endoscope and navigation into difficult-to-reach locations (e.g. the lower pole of the kidney) during lithotripsy, use of small-core fibers (< 200 µm) is necessary. It has been shown that 100-µm-core fibers can deliver up to about 40 W of TFL power while bent to a radius of only 5 mm [42]. The use of a smaller fiber also frees space through the working port of the endoscope so that higher saline irrigation rates can be achieved, as shown in Table 4 of Chapter 5, which will result in more efficient removal of stone dust particles from the surgical field of view and hence a safer procedure. Furthermore, fiber tip degradation can be alleviated through the use of a tapered fiber. The tapered fiber provides advantages of both the large and small core fibers without sacrificing treatment area and durability (See Table 1 in Chapter 5).

Laser lithotripsy is currently performed with single-use, sterile, disposable optical fibers. Although these fibers are standard low-OH silica multimode fibers that can be

purchased at very low cost (e.g. a few dollars per meter) for scientific use, sterile packaged fibers approved for use in the clinic often cost significantly more (e.g. hundreds of dollars per 2 meter fiber). Two major costs associated with these fibers include sterilization required for use in the human body and connectorization at the end of the fiber for attachment and alignment with the laser. These clinical lithotripsy fibers are typically 2 meters in length. Even though only a few millimeters of the fiber may be lost due to "burn-back" during the lithotripsy procedure, the fiber is typically not reused to avoid infection between patients. Also, if the fiber tip is destroyed during a procedure, a new fiber will be used instead of recleaving and polishing the damaged distal fiber tip. Thus, the used fibers are typically disposed of even though the trunk fiber and connectorized end may remain in pristine condition. Considering the fact that laser lithotripsy is the most common laser procedure in urology, with thousands of procedures performed each year, the number of fibers disposed of is significant. The added cost of the disposable fiber also significantly impacts the total cost of the lithotripsy procedure.

An alternative approach to eliminate the need for continuously replacing these expensive "single-use" fibers is to create a more permanent fiber. This permanent fiber could be integrated into an endoscope. If the trunk fiber is integrated into the endoscope, the need for a new fiber would be eliminated because the fiber would be insulated within the endoscope and never become exposed to the body or risk contamination during the procedure. Currently, the endoscope is sterilized after each procedure, so this design would not add any cost to the current procedure. Furthermore, without the need of replacing the fiber, the connectorized end may also be reused, thus eliminating one of the major costs in fiber production. Current lithotripsy procedures using the Ho:YAG laser

prevent the integration of a fiber and endoscope due to the poor, multimodal spatial beam profile of the Ho:YAG laser. However, much smaller core fibers can be used with the TFL (which emits the laser radiation from a fiber core of only 18 μm), and an integrated scope with fiber can be realized. Disposable distal fiber optic tips of varying sizes (100-300 μm) can be attached to the endoscope based on the specific needs of the clinician during an individual lithotripsy case.

The problem with a permanent fiber integrated into the endoscope is that the distal fiber tip rapidly degrades during lithotripsy due to ejected stone fragments impacting the fiber tip. Therefore, we propose a novel approach to solving this problem by designing a detachable and disposable fiber tip. The purpose of this study was to analyze a removable fiber tip design for use in the treatment of urinary stones. The amount of energy transmitted through the system was measured. The energy distribution at the distal end of the fiber tip was compared to that of the tapered fiber. Finally, TFL ablation rates of COM stones using standard pulse trains and MPTs were measured and compared to the tapered fiber.

7.2 Methods

The design used for this study consisted of a 300-μm-core fiber tip attached to a 150-μm-core trunk fiber. The tip was held in place using a spring loaded turn-key lock system as shown in Figure 38. The fiber tip was inserted into a tube connected to the trunk fiber. The spring within the tube holding the fiber tip was compressed. The tip was then rotated so that the key was locked in place. Once the tip was in the fiber, the force from the spring kept a constant push against the fiber tip so that it did not move around during use.

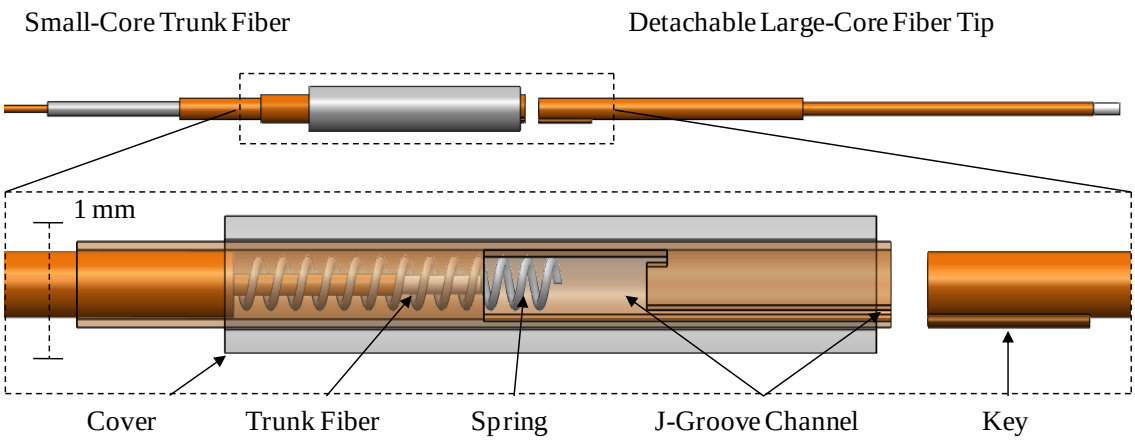

Figure 38. Design of fiber with detachable tip and a close-up view of the spring loaded locking mechanism.

Optical transmission loss through the system was calculated by measuring the power at the proximal and distal ends of the fiber. To determine the cause of any transmission loss, a thermal camera was used to detect leaking infrared energy (Thermovision A20M, FLIR Systems, Boston, MA). The spatial beam profile of energy at the distal end of both the tapered fiber and detachable tip was captured using an infrared camera (Spiricon Pyrocam III, Ophir, Logan, UT).

The ablation study was conducted in the same manner as those in previous chapters. COM stones were held fixed in a saline bath while irradiated by the TFL (n=5 for each study). For each sample, 6000 pulses were delivered. The pulse duration was 500 μs. The pulse energy for each 500 μs pulse was 30 mJ. Experiments were conducted using both tapered fibers and detachable tip fibers. A study was conducted for each of the following pulse trains: a standard 50 Hz train, a standard 100 Hz train, a 10 Hz MPT, and a 20 Hz MPT (MPT profiles shown in Figure 34).

7.3 Results

The transmission through the detachable tip fiber system was 79.9%. The transmission for the tapered fiber was 91.7%. When accounting for an estimated 4% Fresnel loss at each interface, the tapered fiber performed as expected. The detachable tip fiber, on the other hand, transmitted only 93% of the expected power. The remaining power is suspected to have been lost as thermal energy as shown in the thermal distribution of the detachable tip design in Figure 39.

The temperature increases at the interfaces of both the detachable tip and tapered fiber tip are shown in Table 9. Temperature increased with overall increasing power through the system. There was no distinguishable pattern between temperature increases using a standard pulse train versus a MPT. As expected, the largest temperature increases were seen with the detachable tip design. This may be due to the reflections at the interfaces and the greater divergence of the beam exiting the distal end of the detachable tip. The tapered fiber tip showed little temperature increase.

Table 9. Peak temperatures at the distal ends of the trunk and tip of the detachable design and of the tapered fiber tip.

		Detachable Tip		
Pulse Profile	Pulses/sec	Interface	Distal Tip	Tapered Tip
50 Hz	50	30.1 (Δ5.5)	36.1 (Δ11.5)	25.3 (Δ1.9)
10 Hz (Packet)	50	27.8 (Δ3.2)	37.4 (Δ12.8)	25.9 (Δ2.5)
100 Hz	100	31.2 (Δ6.6)	48.5 (Δ23.9)	27.3 (Δ3.9)
20 Hz (Packet)	100	33.5 (Δ8.9)	47.0 (Δ22.4)	27.8 (Δ4.4)

*Estimation based on linear fit of measured temperatures from low pulse rates

The temperature distribution for the detachable tip design is shown in Figure 39.

As expected, there was a temperature increase at the interface between the fiber tip and the trunk fiber as well as the distal end of the fiber tip. The interface temperature increase is noticed at both ends of the hypodermic needle used to encapsulate the system. It is suspected the reason for the larger increase of temperature towards the proximal end of the fiber is due to the back reflection of infrared radiation off the proximal end of the detachable tip toward the distal end of the trunk fiber. The increase in temperature along the length of design is likely due to the properties of the materials used in the design.

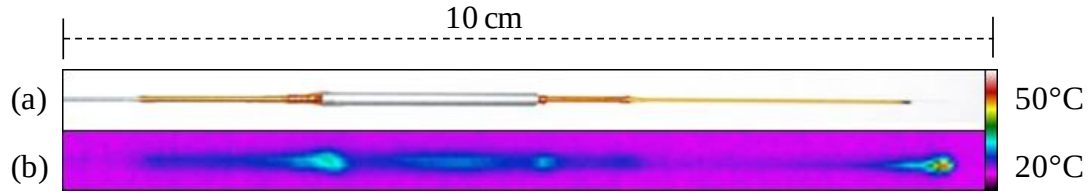

Figure 39. (a) Detachable tip and trunk fiber. (b) Temperature distribution along the length of the interface between the detachable tip and the trunk fiber when operating at 30 mJ, 20 Hz MPTs.

COM stone ablation rates using the detachable tip are shown in Table 10. As expected, the ablation rates using pulse packets was significantly larger than those using standard pulse packets for both the detachable tip design and tapered fiber. The ablation rates using the tapered fiber were slightly less than those using the detachable tip, although this difference was not statistically significant.

Table 10. COM stone ablation rates using the detachable tip and the tapered fiber for different pulse profiles.

Pulse Profile	Pulses/sec	Detachable Tip (μg/s)	Tapered Tip (μg/s)
50 Hz	50	50 ± 15	47 ± 9
10 Hz (Packet)	50	108 ± 13	94 ± 22
100 Hz	100	113 ± 8	92 ± 37
20 Hz (Packet)	100	187 ± 37	175 ± 31

Fiber tip degradation for the parameters used is shown in Figure 40. The detachable tips show no significant damage for the standard pulse trains and the MPT at 10 Hz. However, significant fiber tip damage was observed using the 20 Hz MPT. This may be due to a decrease in time for the ablated area to cool between pulse packets when using the 20 Hz MPT. When operating at 100 Hz, there is 9.5 ms between each 30 mJ pulse. When the pulses are redistributed to operate as a MPT at 20 Hz, there is 45.5 ms between each pulse containing effectively 150 mJ. It is evident that for the 10 Hz MPT, there is sufficient time between pulses to prevent thermal damage to the fiber tip. But at pulse rates higher than that residual thermal damage at the fiber tip is observed.

The tapered fiber was compared using the 20 Hz MPT. The damage to the tapered fiber tip was not evenly distributed, suggesting a concentration of energy at the center of the fiber. This is in line with theory that suggests a beam would be more collimated leaving a distal tapered fiber tip than what was coupled into the proximal trunk fiber as described in Chapter 5. Even though the spatial beam profile is different than that of the detachable tip as shown in Figure 41 data from both this study and that described in Chapter 5 suggests that it does not play a significant role in ablation rates of urinary stones.

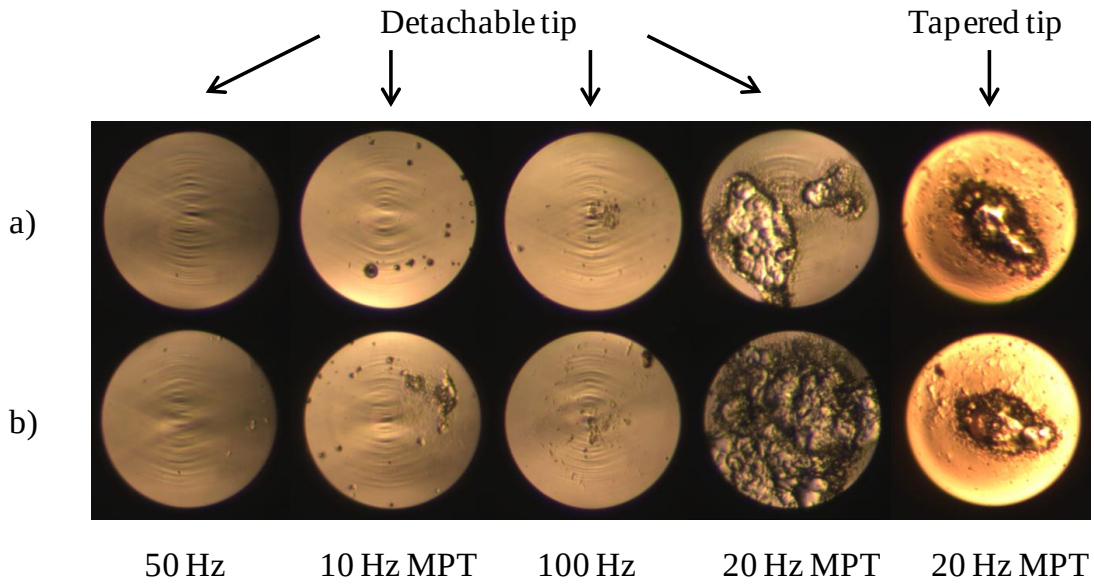

Figure 40. Damage of distal tips after a) 6000 pulses and b) 12000 pulses

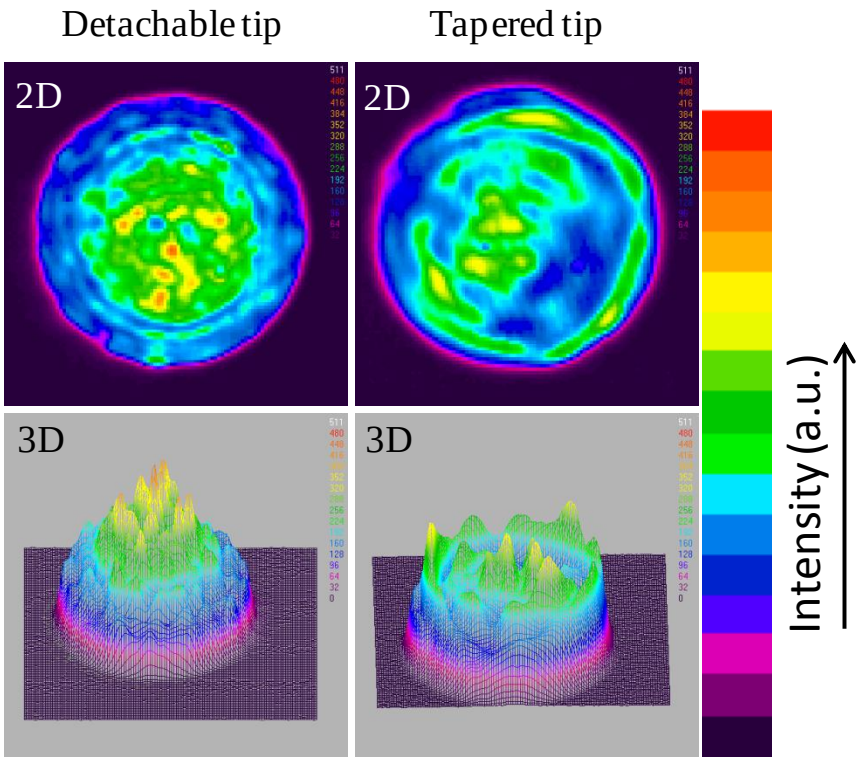

Figure 41. Spatial beam profiles for the detachable and tapered fiber tips.

7.4 Discussion

The motivation for using a detachable fiber tip evolved from conclusions drawn in previous studies of this project. The TFL has the unique ability to couple sufficiently high pulse energy for stone ablation into comparably small fibers to those used in current urinary stone treatment. Our first study found that small-core fibers were able to transfer high amounts of energy with bending radii sufficient to reduce, and possibly eliminate, hindering of ureteroscope deflection. Irrigation rates through the ureteroscope using small fibers were found to be better than those using fibers with larger core diameters. Unfortunately, significant fiber burn-back was observed during the treatment of kidney stones. Although large-core fibers did not have the superior flexibility and irrigation rates of the small-core fibers, they held up better under lithotripsy.

This led us to the idea of using a tapered fiber that combined the benefits of using small-core fibers with those of using large-core fibers. The tapered fiber tip withstood the violent ablation process because of its larger diameter, and was able to maintain a consistent power output due to the lack of damage at the tip. The tapered fiber also proved to be as flexible as and have higher irrigation rates than the small-core fibers, as demonstrated in Chapter 5. The TFL is capable of producing ablation rates comparable to the Ho:YAG using less energy. This allows for the use of a larger core fiber without increasing retropulsion.

Unfortunately, the process of drawing the tapered fiber resulted in an exposed and delicate fiber tip at the beginning of the taper. Because the connection of the tapered tip was delicate, studying the ablation rates using urinary stones was a tedious process to prevent the tip from breaking from the trunk fiber. The precautions taken to avoid

breaking the tip were to move the fiber across the stone by hand, minimizing the force between the fiber and the stone, while still maintaining the closest possible contact. This was likely a large contributor to the sometimes high and inconsistent standard deviations in ablation rates found using the tapered fiber. The lack of durability of the tapered fiber resulted in a lower ablation consistency than that of other types of fibers studied.

Due to the limitations of the tapered fiber, a detachable fiber tip approach was taken. The removable tip would have all the same advantages of the tapered fiber, but the tip would be secured in place using a more robust design. This resulted in higher durability, leading to higher ablation consistency. Furthermore, the design for the removable tip has the potential to be integrated into the ureteroscope. This design would require the trunk fiber to be integrated into the scope in the same manner that the illumination and detection fibers are currently integrated. The design allows for the tip to be removed and discarded after each use. The preservation of the trunk fiber could reduce the costs associated with treatment of kidney stones, as the current process requires new, sterilized, fibers to be used for each treatment. Table 11 compares the properties studied using the small-core, large-core, tapered, and detachable tip fibers.

Table 11. Comparison of small-core, large-core, tapered fibers, and detachable tip fibers for laser lithotripsy.

Properties	Small-core	Large-core	Tapered	Detachable tip
Flexibility	+	-	+	+
Irrigation	+	-	+	+
Power delivery	-	+	+	+
Burnback	-	+	+	+
Durability	-	+	-	+
Reusability	-	-	-	+
Ablation Consistency	+	+	-	+

This study demonstrated that using a detachable fiber tip did not cause a decrease in ablation rates compared to previous studies using standard and tapered fiber tips, and that the design for a detachable tip is durable enough to withstand the temperatures and stone particle expulsion that could lead to design failure. Furthermore, the results using the detachable fiber tip were more consistent than those using the tapered fibers, implying that the design is able to withstand being pressed against the stone without breaking the tip or decreasing power delivery. The limitations of the TFL did not allow for higher pulse energies to be explored, but further exploration with pulse modulation may prove higher pulse energies to be unnecessary.

One point of concern is the temperature distribution along the fiber tip design. Energy being delivered in the body during kidney stone treatment would ideally be confined to the point of contact with the stone and fiber tip. Additional studies with different detachable designs and materials could eliminate this problem. Also, the temperature increase may not be significant, but this is subjective to the surgeon and dependent upon the tolerances of the ureteroscope being used. Reduction or possible

elimination of energy transmission loss at the interface between the trunk and the fiber tip would be most desirable.

7.5 Conclusion

Previous chapters demonstrate the advantages of using both small-core and large-core fibers. The tapered fiber studies combined the advantages of the two fibers, and were shown to be a viable alternative to conventional fibers. The use of a detachable fiber tip builds on the advantages of the tapered fiber to give a more stable and reusable alternative design. Furthermore, the detachable fiber tip design has the potential to be integrated into a flexible endoscope, which would greatly reduce costs associated with replacing optical fibers for urinary stone treatment.

CHAPTER 8: CONCLUSIONS

These research studies demonstrate the potential advantages of the Thulium fiber laser for lithotripsy. The TFL has an excellent spatial beam profile that allows it to couple higher laser power into smaller fibers than those currently used for lithotripsy. This in turn allows for better irrigation and higher flexibility of the endoscope during the procedure.

If the urologist is concerned about minimizing stone retropulsion, then the TFL provides an alternative to the Ho:YAG laser. Previous studies reporting on the optimal set of Ho:YAG laser parameters for efficient lithotripsy with minimal stone retropulsion have reached similar conclusions, namely that Ho:YAG laser operation with lower pulse energies and higher pulse rates than currently used in the clinic would also be beneficial. Recent Ho:YAG laser lithotripsy retropulsion studies have also concluded that use of lower pulse energies, longer pulse durations, higher pulse rates, and smaller optical fiber diameters is the optimal combination for minimizing stone retropulsion [35-40]. Unlike the flashlamp-pumped Ho:YAG laser, the diode-pumped TFL is an ideal laser for operation with this range of laser parameters, due to the TFL's excellent spatial beam profile which allows use of small-core fibers and its operation at arbitrary pulse durations and pulse rates.

In addition to reducing retropulsion, this study has demonstrated that operating at a wavelength more highly absorbed by water decreases the ablation threshold of both UA

and COM stones by a factor of four. Furthermore, operating at higher TFL pulse rates at this low energy result in comparable ablation of urinary stones to that of the conventional Ho:YAG. While the trend of this research is promising, further studies with higher TFL pulse energy should be conducted to further explore the viability of the TFL to ablate stones as efficiently as the Ho:YAG in a clinical setting.

The exploitation of the TFL for urinary stone ablation is not only promising because it may alleviate troubles plaguing current Ho:YAG lithotripsy; it also opens the door to new possibilities for treatment of urinary stones. Because the TFL is externally modulated with a function generator, more complex pulse train delivery is possible. Preliminary research presented in Chapter 6 demonstrates the ability of MPTs to out-perform standard pulse trains delivering the same power to the stone. Retropulsion, charring, and heating of surrounding water/tissue is a result of energy wasted. Conducting more extensive research on complex pulse trains may yield even better results that would eliminate wasted energy, while increasing the efficiency and safety of the treatment of urinary stones.

In addition to unique pulse delivery, the TFL is better suited to utilize the suction effect reported in this research. Utilization of this phenomenon may not only reduce or eliminate retropulsion, but has the potential to be used as a tool for stone manipulation within the urinary tract. This would eliminate the need for space consuming stone grasping tools and give the surgeon more control of stone positioning during ablation.

Because of the unique ability of the TFL to couple energy into small fibers with minimal energy loss or fiber damage [42], this research has explored the use of unconventional fibers for laser lithotripsy. The tapered fiber is an alternative to

large/small-core fibers that exploits maximum saline irrigation and smaller bending radii without sacrificing the robustness of a large-core tip. Keeping with the advantages of the tapered fiber, but realizing the delicacy of the taper-trunk interface, a detachable tip fiber was designed. The results in the treatment of urinary stones using this design were comparable to that of the tapered fiber, giving the added benefit of replacing just the tip should the fiber become damaged. Further studies should be conducted to minimize energy loss at the trunk-tip interface of the detachable tip fiber.

This research has demonstrated the potential of the Thulium fiber laser to replace the conventional Holmium:YAG for the treatment of urinary stones. The better water absorption at the TFL wavelength, superior spatial beam profile, and flexibility in the temporal beam profile make it an ideal candidate to address current problems with laser lithotripsy and add to the existing technology.

REFERENCES

[1] M. S. Pearle, *et al.*, "Urologic diseases in America project:Urolithiasis," *Journal of Urology,* vol. 173, pp. 848-857, Mar 2005.

[2] C. S. Saigal, *et al.*, "Direct and indirect costs of nephrolithiasis in an employed population: Opportunity for disease management?," *Kidney International,* vol. 68, pp. 1808-1814, Oct 2005.

[3] J. M. Soucie, *et al.*, "Relation between geographic variability in kidney stones prevalence and risk factors for stones," *American Journal of Epidemiology,* vol. 143, pp. 487-495, Mar 1996.

[4] T. H. Brikowski, *et al.*, "Climate-related increases in the prevalence of urolithiasis in the United States," in *National Academy of Science,* 2008, pp. 9841-9846.

[5] D. M. Wilson, "Clinical and laboratory approaches for evaluation of nephrolithiasis," *Journal of Urology,* vol. 141, pp. 770-774, Mar 1989.

[6] B. Struve and G. Huber, "Properties and medical applications of near-IR solid-state lasers," *Journal De Physique Iv,* vol. 1, pp. 3-6, Dec 1991.

[7] T. D. White, *et al.*, "Evaluation of retropulsion caused by Holmium:YAG laser with various power settings and fibers," *Journal of Endourology,* vol. 12, pp. 183-186, Apr 1998.

[8] H. Lee, *et al.*, "Stone retropulsion during Holmium:YAG lithotripsy," *Journal of Urology,* vol. 169, pp. 881-885, Mar 2003.

[9] D. S. Finley, *et al.*, "Effect of Holmium:YAG laser pulse width on lithotripsy retropulsion in vitro," *Journal of Endourology,* vol. 19, pp. 1041-1044, Oct 2005.

[10] C. G. Marguet, *et al.*, "In vitro comparison of stone retropulsion and fragmentation of the frequency doubled, double pulse Nd:Yag laser and the Holmium:Yag laser," *Journal of Urology,* vol. 173, pp. 1797-1800, May 2005.

[11] H. W. Kang, *et al.*, "Dependence of calculus retropulsion on pulse duration during Holmium:YAG laser lithotripsy," *Lasers in Surgery and Medicine,* vol. 38, pp. 762-772, Sep 2006.

[12] P. Kalra, *et al.*, "Effect of pulse width on object movement in vitro using Holmium:YAG laser," *Journal of Endourology,* vol. 21, pp. 228-231, Feb 2007.

[13] S. Griffin, "Fiber optics for destroying kidney stones," in *Biophotonics International*, 2004, pp. 44-47.

[14] G. M. Hale and M. R. Querry, "Optical-constants of water in 200-nm to 200-Mm wavelength region," *Applied Optics*, vol. 12, pp. 555-563, 1973.

[15] E. D. Jansen, *et al.*, "Temperature-dependence of the absorption-coefficient of water for midinfrared laser-radiation," *Lasers in Surgery and Medicine*, vol. 14, pp. 258-268, 1994.

[16] B. I. Lange, *et al.*, "Temperature dependence of light absorption in water at Holmium and Thulium laser wavelengths," *Applied Optics*, vol. 41, pp. 5797-5803, Sep 2002.

[17] K. T. Schomacker, *et al.*, "Co:MgF2 Laser ablation of tissue- effect of wavelength on ablation threshold and thermal-damage," *Lasers in Surgery and Medicine*, vol. 11, pp. 141-151, 1991.

[18] F. A. Duck, *Physical properties of tissue: A comprehensive reference network*. Bath, England: Academic Press, 1990.

[19] K. R. Holmes, " Thermal conductivity data for specific tissues and organs for humans and other mammalian species," University of Texas at Austin, Austin, TX, 2013.

[20] K. F. Chan, *et al.*, "Free electron laser lithotripsy: Threshold radiant exposures," *Journal of Endourology*, vol. 14, pp. 161-167, Mar 2000.

[21] A. Roggan, *et al.*, *"Properties of biological tissues" in Applied laser Medicine*. Berlin: Springer-Verlag, 2003.

[22] S. S. Spore, *et al.*, "Holmium:YAG lithotripsy: Optimal power settings," *Journal of Endourology*, vol. 13, pp. 559-566, Oct 1999.

[23] L. Jonat, *et al.*, "Ho:YAG lithotripsy fragmentation varies with pulse energy," in *Engineering in urology Society Annual Meeting*, 2010, p. 84.

[24] M. Frenz, *et al.*, "Comparison of the effects of absorption coefficient and pulse duration of 2.12-mm and 2.79-mm radiation on laser ablation of tissue," *Ieee Journal of Quantum Electronics*, vol. 32, pp. 2025-2036, Dec 1996.

[25] T. Asshauer, *et al.*, "Pulsed holmium laser ablation of tissue phantoms: correlation between bubble formation and acoustic transients," *Applied Physics B-Lasers and Optics*, vol. 65, pp. 647-657, Oct 1997.

[26] F. Wezel, *et al.*, "Effect of pulse energy, frequency and length on holmium: yttrium-aluminum-garnet laser fragmentation efficiency in non-floating artificial urinary calculi," *Journal of Endourology*, vol. 24, pp. 1135-1140, Jul 2010.

[27] PubMed. *Kidney Stones*. Available: http://www.ncbi.nlm.nih.gov/pubmedhealth/PMH0001493/, Feb 15, 2013.

[28] H. Lee, *et al.*, "Dependence of calculus retropulsion dynamics on fiber size and radiant exposure during Ho:YAG lithotripsy," *Journal of Biomechanical Engineering-Transactions of the Asme,* vol. 126, pp. 506-515, Aug 2004.

[29] P. Zhong, *et al.*, "Transient cavitation and acoustic emission produced by different laser lithotripters," *Journal of Endourology,* vol. 12, pp. 371-378, Aug 1998.

[30] J. W. Dushinski and J. E. Lingeman, "High-speed photographic evaluation of holmium laser," *Journal of Endourology,* vol. 12, pp. 177-181, Apr 1998.

[31] K. F. Chan, *et al.*, "A perspective on laser lithotripsy: The fragmentation processes," *Journal of Endourology,* vol. 15, pp. 257-273, Apr 2001.

[32] K. F. Chan, *et al.*, "Holmium : YAG laser lithotripsy: A dominant photothermal ablative mechanism with chemical decomposition of urinary calculi," *Lasers in Surgery and Medicine,* vol. 25, pp. 22-37, 1999.

[33] G. J. Vassar, *et al.*, "Holmium : YAG lithotripsy: Photothermal mechanism," *Journal of Endourology,* vol. 13, pp. 181-190, Apr 1999.

[34] S. Pierre and G. M. Preminger, "Holmium laser for stone management," *World Journal of Urology,* vol. 25, pp. 235-239, Jun 2007.

[35] J. C. Sung, *et al.*, "Location and etiology of flexible and semirigid ureteroscope damage," *Urology,* vol. 66, pp. 958-963, Nov 2005.

[36] F. Pasqui, *et al.*, "Impact on active scope deflection and irrigation flow of all endoscopic working tools during flexible ureteroscopy," *European Urology,* vol. 45, pp. 58-64, Jan 2004.

[37] O. A. Nazif, *et al.*, "Review of laser fibers: A practical guide for urologists," *Journal of Endourology,* vol. 18, pp. 818-829, Nov 2004.

[38] A. J. Marks, *et al.*, "Holmium:Yttrium-Aluminum-Garnet lithotripsy proximal fiber failures from laser and fiber mismatch," *Urology,* vol. 71, pp. 1049-1051, Jun 2008.

[39] A. C. Mues, *et al.*, "Quantification of Holmium:Yttrium Aluminum Garnet Optical Tip Degradation," *Journal of Endourology,* vol. 23, pp. 1425-1428, Sep 2009.

[40] A. C. Mues, *et al.*, "Evaluation of 24 Holmium:YAG Laser Optical Fibers for Flexible Ureteroscopy," *Journal of Urology,* vol. 182, pp. 348-354, Jul 2009.

[41] J. P. Clarkin, *et al.*, "Shaped fiber tips for medical and industrial applications," in *Proc. SPIE*, 2004, pp. 70-80.

[42] N. J. Scott, *et al.*, "Thulium Fiber Laser Ablation of Urinary Stones Through Small-Core Optical Fibers," *IEEE Journal of Selected Topics in Quantum Electronics*, vol. 15, pp. 435-440, Mar-Apr 2009.

[43] C. Abdelshehid, *et al.*, "Comparison of flexible ureteroscopes: Deflection, irrigant flow and optical characteristics," *Journal of Urology*, vol. 173, pp. 2017-2021, Jun 2005.

[44] G. J. Vassar, *et al.*, "Holmium:YAG lithotripsy efficiency varies with energy density," *Journal of Urology*, vol. 160, pp. 471-476, Aug 1998.

[45] B. E. Knudsen, *et al.*, "Performance and safety of Holmium:YAG laser optical fibers," *Journal of Endourology*, vol. 19, pp. 1092-1097, Nov 2005.

[46] C. J. Pagnani, *et al.*, "Prevention of Stone Migration with the Accordion During Endoscopic Ureteral Lithotripsy," *Journal of Endourology*, vol. 26, pp. 484-488, May 2012.

[47] C. D. Ohl, *et al.*, "Bubble dynamics, shock waves and sonoluminescence," *Philosophical Transactions of the Royal Society of London Series a-Mathematical Physical and Engineering Sciences*, vol. 357, pp. 269-294, Feb 1999.

[48] A. A. Buzak and V. S. Teslenko, "Sonoluminescense following focusing of laser radiation into liquid," *Journal of Experimental and Theoretical Physics*, vol. 14, pp. 189-191, 1971 1971.

[49] K. F. Chan, *et al.*, "Erbium:YAG laser lithotripsy mechanism," *Journal of Urology*, vol. 168, pp. 436-441, Aug 2002.

[50] T. Lu, *et al.*, "Cavitation effect of holmium laser pulse applied to ablation of hard tissue underwater," *Journal of Biomedical Optics*, vol. 15, Jul-Aug 2010.

[51] T. Asshauer, *et al.*, "Acoustic transient generation by holmium-laser-induced cavitation bubbles," *Journal of Applied Physics*, vol. 76, pp. 5007-5013, Nov 1994.

[52] B. Han, *et al.*, "Mechanical effects of laser-induced cavitation bubble on different geometrical confinements for laser propulsion in water," *Optics and Lasers in Engineering*, vol. 49, pp. 428-433, Mar 2011.

[53] E. A. Brujan, *et al.*, "The final stage of the collapse of a cavitation bubble close to a rigid boundary," *Physics of Fluids*, vol. 14, pp. 85-92, Jan 2002.

[54] A. Vogel and W. Lauterborn, "Acoustic transient generation by laser-produced cavitation bubbles near solid boundaries," *Journal of the Acoustical Society of America,* vol. 84, pp. 719-731, Aug 1988.

[55] A. Brujan and Y. Matsumoto, "Collapse of micrometer-sized cavitation bubbles near a rigid boundary," *Microfluidics and Nanofluidics,* vol. 13, pp. 957-966, 2012.

[56] S. T. Hendow, *et al.*, "Percussion drilling of metals using bursts of nanosecond pulses," *Optics Express,* vol. 19, pp. 10221-10231, May 2011.

[57] A. Vogel, *et al.*, "Minimization of thermomechanical side effects in IR ablation by use of multiple q-switched laser pulses," *Medical Laser Applications,* vol. 17, pp. 15-20, 2002.

[58] D. P. Joseph, *et al.*, "A new and improved vitreoretinal Erbium:YAG laser scalpel: Long-term morphologic characteristics of retinal-choroidal injury," *Ophthalmic Surgery Lasers & Imaging,* vol. 35, pp. 304-315, Jul-Aug 2004.

[59] F. Pohl, *et al.*, "Influence of Ho:YAG pulse modification on in vitro stone disintegration," *Journal of Endourology,* vol. 25, pp. A-42, 2011.

[60] M. Frenz, *et al.*, "Starting mechanisms and dynamics of bubble formation induced by a Ho:Yttrium aluminum garnet laser in water," *Journal of Applied Physics,* vol. 84, pp. 5905-5912, Dec 1998.

APPENDIX A: PEER REVIEWED JOURNAL ARTICLES

[1] T.C. Hutchens, **R. L. Blackmon**, P. B. Irby, and N. M. Fried, "Detachable Fiber Optic Tips for use in Thulium Fiber Lithotripsy," *Journal of Biomedical Optics*, In Press.

[2] **Blackmon RL**, Case JR, Trammell SR, Irby PB, Fried NM. Fiber optic manipulation of urinary stone phantoms using Holmium:YAG and Thulium fiber lasers. *Journal of Biomedical Optics* 18(2):028001, 2013.

[3] **R. L. Blackmon**, P. B. Irby, and N. M. Fried, "Enhanced thulium fiber laser lithotripsy using micro-pulse train modulation," *Journal of Biomedical Optics*, vol. 17, issue 2, Feb 2012.

[4] **R. L. Blackmon**, P. B. Irby, and N. M. Fried, "Comparison of Holmium:YAG and Thulium fiber laser lithotripsy: ablation thresholds, ablation rates, and retropulsion effects," *Journal of Biomedical Optics*, vol. 16, issue 7, July 2011.

[5] **R. L. Blackmon**, P. B. Irby, and N. M. Fried, "Holmium:YAG (λ=2,120nm) Versus Thulium Fiber (λ=1,908nm) Laser Lithotripsy," *Lasers in Surgery and Medicine*, vol. 42, pp. 232-236, Mar 2010.

[6] **R. L. Blackmon**, P. B. Irby, and N. M. Fried, "Thulium Fiber Laser Lithotripsy Using Tapered Fibers," *Lasers in Surgery and Medicine*, vol. 42, pp. 45-50, Jan 2010.

APPENDIX B: CONFERENCE PROCEEDINGS

[1] **R. L. Blackmon**, P. B. Irby, and N. M. Fried, " Comparison of Thulium Fiber Laser and Holmium:YAG Laser for Fiber Optic Manipulation of Urinary Stone Phantoms," *Proc. SPIE*, vol. 8565, 2013.

[2] T.C. Hutchens, **R. L. Blackmon**, P. B. Irby, and N. M. Fried, "T.C. Hutchens, R. L. Blackmon, P. B. Irby, and N. M. Fried, "Detachable Fiber Optic Tips for use in Thulium Fiber Lithotripsy," *Proc. SPIE*, vol. 8565, 2013.

[2] **R. L. Blackmon**, P. B. Irby, and N. M. Fried, "Improved thulium fiber laser vaporization of urinary stones using micro-pulse packets," *Proc. SPIE*, vol. 8207, 2012.

[3] **R. L. Blackmon**, P. B. Irby, and N. M. Fried, "Comparison of Holmium:YAG and Thulium fiber laser lithotripsy: ablation thresholds, ablation rates, and retropulsion effects," *Proc. SPIE*, vol. 7914, 2011.

[4] N. M. Fried, **R. L. Blackmon**, and P.B. Irby, "A review of Thulium fiber laser ablation of kidney stones," *Proc. SPIE*, vol. 7914, 2011.

[5] **R. L. Blackmon**, P. B. Irby, and N. M. Fried, "Comparison of Holmium:YAG and Thulium fiber lasers for lithotripsy," *Proc. SPIE*, vol. 7548, 2010.

[6] **R. L. Blackmon**, P. B. Irby, and N. M. Fried, "A tapered distal fiber tip for Thulium fiber laser lithotripsy," *Proc. SPIE*, vol. 7548, 2010.

[7] **R. L. Blackmon**, P. B. Irby, and N. M. Fried, "Holmium:YAG laser lithotripsy at high pulse energies versus Thulium fiber laser lithotripsy at high pulse rates," Engineering in Urology Society Annual Meeting (Abstract #72), p. 86, 2010.

APPENDIX C: PATENTS

[1] N. M. Fried, **R. L. Blackmon**, P. B. Irby, T.C. Hutchens, "Novel endoscope tube with detachable fiber tips," Provisional U.S. patent filed, Application # 61/296,921, Jan. 2010.